Results in Optics 5 (2021) 100196

Contents lists available at ScienceDirect

Results in Optics

journal homepage: www.sciencedirect.com/journal/results-in-optics

Invited Article

(INVITED)Chemical sensors based on long period fiber gratings: A review

Flavio Esposito

Department of Engineering, University of Naples "Parthenope", Centro Direzionale Isola C4, 80143 Napoli, Italy

ARTICLE INFO

Keywords:
Chemical sensors
Fiber optic sensors
Gas sensors
Long period gratings
Optical sensors

ABSTRACT

Fiber optic devices are being increasingly employed in the fields of chemical and environmental sensing due to their important features, such as high accuracy, small size, chemical inertness, remote operation and multiplexing capabilities. In this work, a thorough review about the design, fabrication and characterization of fiber optic chemical sensors based on long period grating (LPG) technology is reported. The emphasis is placed on transducer designs and features as well as the techniques to enhance the sensitivity. Subsequently, coating materials to be deposited around the grating region, providing a selective response to the target analytes are described in detail. Finally, the different applications are reviewed, mainly related to the monitoring of environmental parameters, volatile organic compounds, hazardous gases, heavy metal ions, corrosion, marine salinity and food quality. The aim of this work is to deliver a comprehensive analysis regarding the state-of-the-art solutions about LPG-based chemical sensors and to summarize the current shortcomings and upcoming research paths.

1. Introduction

Nowadays, optical detection methods represent high-performance solutions for the measurement of various chemical and biological species, achieving very low limits of detection (LOD). A strong impulse is provided by the advancements in the development of functional materials and fabrication processes. The working principles can be based on fluorescence, absorption, luminescence, Raman, refractive index (RI), surface plasmon resonance (SPR) and others (McDonagh et al., 2008).

In this context, fiber optic sensors are valuable and flexible platforms for the development of chemical sensors, due to their numerous advantages, such as small size and weight, no electromagnetic interference, chemical inertness, remote and multiplexed detection capabilities (Wang and Wolfbeis, 2020). As the light propagation into an optical fiber is well confined within the core region, based on the total internal reflection phenomenon, it is necessary to develop structures able "to disturb" such propagation and enable the interaction of the light with the surrounding medium (Urrutia et al., 2019). Consequently, the role of the fiber transducers is to exhibit strong sensitivities to the changes, typically in the RI, occurring on the surface and converting them into an optical signal. Such surface is usually coated with a sensitive material with the ability to selectively interact with the target analyte, which in turn modifies its optical properties (mainly RI and thickness).

It is worth mentioning several high sensitivity transducers which were employed till now for chemical sensing, such as fiber interferometers (Khan et al., 2020; Miliou, 2021), etched/tilted fiber Bragg gratings (FBG) (Guo et al., 2016; Iadicicco et al., 2005), long period gratings (LPG) (Korposh et al., 2017; Zhao and Wang, 2019), surface plasmon resonance (SPR) devices (Liu and Peng, 2021; Sharma et al., 2018) and lossy mode resonance (LMR) sensors (Chiavaioli and Janner, 2021; Vitoria et al., 2021).

In this work, a comprehensive report regarding the state-of-the-art solutions about long period grating-based chemical sensors is presented. All the aspects about the development of chemical sensors have been considered herein, by providing a detailed analysis regarding the fiber transducers and methodologies to enhance the sensitivity, as well as the coating materials providing selectivity to the specific target analytes. The following of the work is organized in this fashion: Section 2 summarizes the working principle of LPG, sensitivity enhancement techniques and main materials used for chemical sensing; Section 3 illustrates the applications to the detection of environmental parameters, volatile organic compounds (VOCs), hazardous gases, heavy metal ions, corrosion, marine salinity, food quality and more; finally, Section 4 provides a conclusion and outlines future research trends.

2. Design of LPG-based chemical sensors

A schematic picture of an LPG-based chemical sensor is reported in Fig. 1. It is composed by an LPG transducer written into an optical fiber, with enhanced sensitivity to the surrounding medium refractive index

E-mail addresses: flavio.esposito@collaboratore.uniparthenope.it, flavio.esposito@uniparthenope.it.

https://doi.org/10.1016/j.rio.2021.100196
Received 31 August 2021; Received in revised form 25 October 2021; Accepted 17 November 2021
Available online 22 November 2021

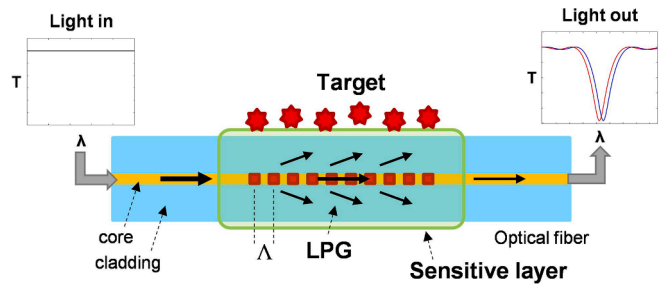

Fig. 1. Schematic representation of fiber optic chemical sensor composed by an LPG coated with a sensitive material for the capture of the target analyte.

(SRI). Moreover, to provide the sensor with selective response to specific target analytes, it is coated with a material exhibiting a change in its own optical properties in response to the target. In some conditions, such material can be also designed to enhance the bulk RI sensitivity of the transducer. The details regarding the working principle of LPG, sensitivity enhancement techniques and coating materials for chemical sensing are reported in the following.

2.1. Long period grating: Working principle and overview

The LPG is an optical fiber component which is fabricated by inducing a periodic perturbation in the refractive index (and sometimes geometry) into an unjacketed portion of an optical fiber. The period of the perturbation Λ typically ranges from 100 μm to 1 mm and enables the power coupling between the fundamental mode propagating in the core and co-propagating cladding modes, as schematically illustrated in Fig. 1. Such coupling is wavelength selective and the fiber transmission spectrum presents several dips associated to different cladding modes (see Light out in Fig. 1), whose resonance wavelengths are given by the following phase-matching condition:

$\lambda_{res,i} = \left(n_{eff,co} - n_{eff,cl}^{(i)}\right) \bullet \Lambda$; where $n_{eff,co}$ and $n_{eff,cl}^{(i)}$ are the effective refractive indices of the core and ith cladding mode, respectively, while Λ is the grating periodicity. The transmission value of the attenuation bands at resonance wavelengths is then given by: $T_i = \cos^2(k_i \bullet L)$; where k_i is the coupling coefficient for the ith cladding mode and L is the grating length (James and Tatam, 2003).

An important feature of the LPG is that the resonance wavelength and amplitude of the attenuation bands are dependent upon the external conditions to which the fiber is subjected, through the dependence of the phase-matching condition upon core and cladding effective refractive indices. They can be used to measure, for example, temperature (Shu et al., 2001; Wang et al., 2020b), strain (Del Villar et al., 2018), bending (Allsop et al., 2006; Ren et al., 2017), torsion (Subramanian et al., 2018) and, above all, SRI (Esposito et al., 2021c; Shu et al., 2002) through the variations of cladding mode effective refractive indices with SRI. Therefore, LPGs have found wide application in different sensing domains, like physical (Esposito et al., 2020a, 2019c; Stăncălie et al., 2018), chemical (Korposh et al., 2017) and biological (Chiavaioli et al., 2017a, 2015; Esposito et al., 2021c; Piestrzyńska et al., 2019).

Their fabrication can be achieved using UV laser based techniques and non-UV techniques, as those based on CO_2 lasers (Liu et al., 2018), IR femtosecond lasers (Heck et al., 2019; Viveiros et al., 2021) and electric arc discharge (Esposito et al., 2018a; Rego, 2016; Rego et al., 2021). As the UV methods ensure high repeatability and possibility to achieve very short periods, the latter techniques easily enable the fabrication even in fibers with unconventional compositions and geometrical designs, as for example: pure-silica core fibers (Rego et al., 2005b), rare-earth and specialty doped fibers (Durr et al., 2005; Esposito et al., 2019a; Ranjan et al., 2017; Rego et al., 2005a), polarization-maintaining fibers (PMF) (Esposito et al., 2019b; Jiang et al., 2019), photonic crystal fibers (PCF) (Iadicicco et al., 2015; Srivastava et al., 2019; Zhang et al., 2018), D-shaped fibers (Quero et al., 2011), microchanneled fibers (Srivastava et al., 2020), multimode (MMF) and plastic fibers (Theodosiou et al., 2019). These unconventional configurations can be used to increase the sensitivity or add intriguing features to current applications.

2.2. Sensitivity enhancement techniques

Different approaches have been investigated so far to enhance the SRI sensitivity of LPGs and meet the requirements of chemical and biological applications.

The period of the grating can be designed such that the higher order cladding modes are close to the turn-around point (TAP) of their phase-matching curves (i.e., resonance wavelength and period relationship). When the grating period is slightly lower than that corresponding to a TAP, two resonance bands associated to the coupling with the same cladding mode can be observed in the LPG spectrum. As the period is increased towards TAP, the two peaks progressively merge into a single wide band, as illustrated in Fig. 2. Since the slope of the phase-matching curves approaches infinity around TAP, such point defines the maximum sensitivity condition for each cladding mode. The phenomenon is strongly dependent on the fiber properties, SRI and cladding mode order: it occurs at longer wavelengths for lower order ones and moves to shorter wavelengths when the mode order increases.

The refractometric sensitivity at TAP can reach even thousands of nm/RIU (refractive index unit) (Shu et al., 2002). However, as a general point of view, such working point can be achieved with low period values that can only be obtained with well assessed fabrication methods. The design of the grating period is usually assisted by numerical modeling, moreover in practice the tuning of the working point can be also favorited by cladding etching (Chen et al., 2007; Del Villar et al., 2016; Dey et al., 2021).

The mode transition (MT) phenomenon can be induced by coating a standard optical fiber (e.g., core and cladding) with a material having refractive index higher than cladding (HRI) and appropriate thickness (Cusano et al., 2006a; Del Villar et al., 2005). The presence of an HRI overlay modifies the effective refractive indices of the cladding modes and thus their field distributions. Specifically, for a given SRI value, a set of values for the couple overlay RI and overlay thickness exists inducing mode transition from cladding to overlay (i.e., the mode is confined in the HRI layer with an effective refractive index higher than cladding RI). The consequence is a simultaneous variation of the effective refractive indices of all cladding modes, which in turn produces a shift in the

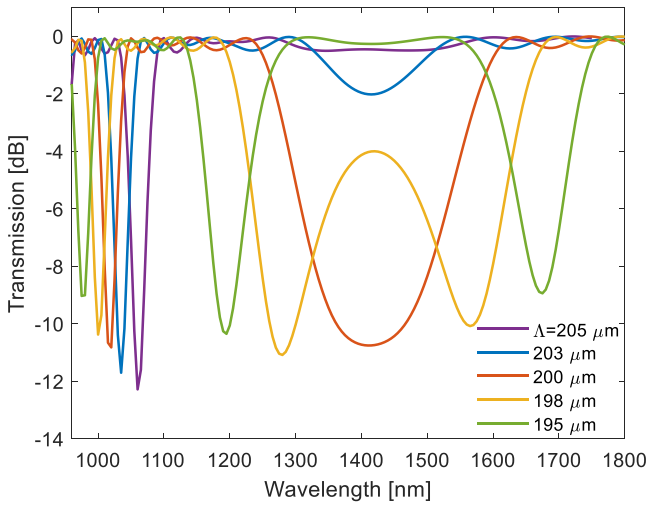

Fig. 2. Transmission spectra of an LPG as a function of the grating period Λ around TAP region.

corresponding attenuation bands. The higher is the cladding mode order, the higher will be the shift. As an example, the effects on grating spectrum and resonance wavelengths of the deposition of a HRI material are reported in Fig. 3(a) and 3(b), respectively. Here, an abrupt change of the resonance wavelengths can be observed during transition, corresponding to an enhanced sensitivity of the LPG to external parameters. The sensor design involves the proper selection of the overlay RI and thickness to maximize the sensitivity with respect to the SRI of the specific application and is usually assisted by numerical simulations. Several materials have been investigated as HRI coatings so far, ranging from polymers to metal oxides with different deposition techniques (Coelho et al., 2016; Esposito et al., 2018b; Quero et al., 2016; Zou et al., 2020).

In the case of MT, the phenomenon can be also induced in LPGs with high periods, even if sensitivity will be lower in such cases. Finally, sensitivities can reach thousands of nm/RIU but the necessity to deposit an additional material onto the fiber must be considered.

Very recently, the possibility to induce mode transition into a double cladding fiber (DCF) with W-shaped RI profile, without any additional HRI overlay, has been also demonstrated. Here, the working point of the device is tuned to transition region by etching the fiber outer diameter (Esposito et al., 2021a; Esposito et al., 2021b; Esposito et al., 2020b). The benefits are the simplicity and long-term stability at cost of lower sensitivity in comparison to HRI coated LPGs.

Useful features for sensing applications can be also achieved by unconventional grating designs and cascaded gratings, as those investigated in (Arjmand et al., 2016; Chiavaioli et al., 2017b, 2013; Pilla et al., 2008). Finally, the previous approaches of TAP and MT are usually combined in order to lift the sensitivity values up to tens of thousands nm/RIU, even if an extremely fine tuning of the working point is necessary in these cases, as reported in (Del Villar, 2015; Pilla et al., 2012; Śmietana et al., 2016).

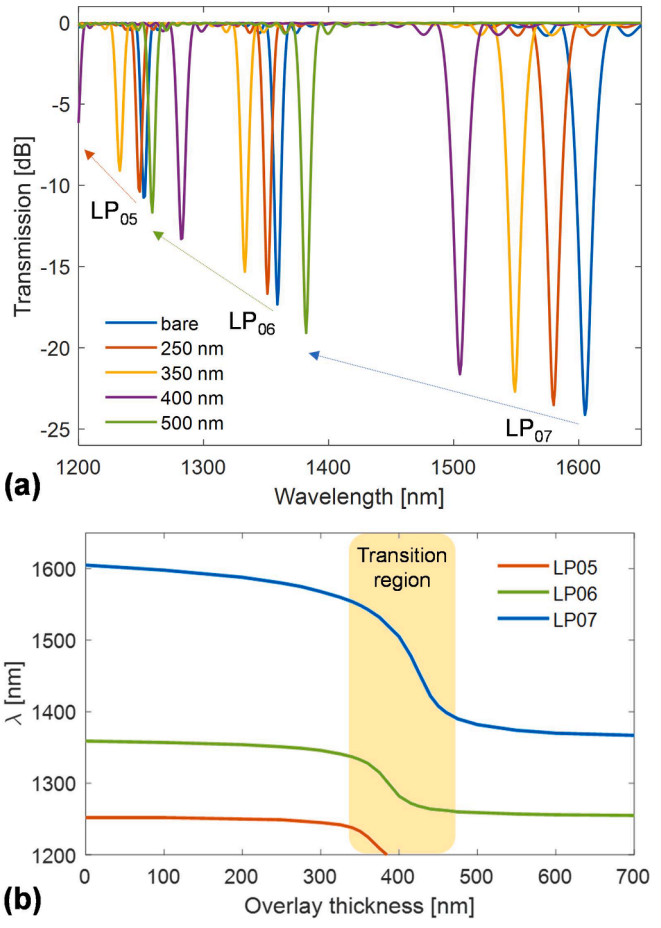

Fig. 3. Mode transition in an LPG coated with an overlay with refractive index of 1.55: (a) Transmission spectra as a function of the overlay thickness; (b) Resonance wavelengths versus overlay thickness.

Overall, LPG based refractometers can provide high sensitivities, however they exhibit wider attenuation bands than other fiber sensors. Cross sensitivities to temperature, strain and bending must be also carefully considered. Interferometric sensors can also obtain good sensitivities, but their insertion losses may be high and it is important to tune the range of unambiguous RI detection (Eftimov et al., 2020). FBG sensors have lower sensitivity but they benefit from reflection configuration. Tilted and etched FBGs have higher sensitivities but fragility increases for the latter (Iadicicco et al., 2005; Lobry et al., 2021). SPR and LMR based sensors need etched, polished or tapered fibers but can provide high sensitivities, even if their resonances are usually wide (Zubiate et al., 2019). Finally, the so-called Lab on Tip/Fiber sensors are worthy to be mentioned due to reflection configuration (Vaiano et al., 2016).

2.3. *Sensitive materials*

To provide LPG transducers with selectivity to a given analyte, they need to be coated with a sensitive material exhibiting changes in its own properties (typically refractive index and/or thickness) in presence of the target. The deposition of the material, as well as its variations, influence the cladding mode distribution and thus the phase-matching condition. Finally, the thickness, size, shape, surface area and porosity of the materials are crucial, since they will affect the device characteristics (e.g., sensitivity, repeatability, response and recovery times).

Polymers have been widely investigated as sensing layers for LPG transducers, due to the possibility of tailoring their chemical and physical properties over a wide range. For example, polyelectrolyte materials show selectivity to several species. They exhibit ionizable functional groups forming charged poly-ions. Among them, for example, poly(allylamine hydrochloride) (PAH) and poly(diallyidimethyl) ammonium chloride (PDDA) are used as polycations with positively charged functional groups (i.e., quaternary ammonium or amino groups), whereas poly(sodium 4-styrene sulfonate) (PSS) and poly (acrylic acid) (PAA) usually serve as polyanions (with sulfonic acids or carboxylic acids). The deposition process involves sequential steps where cationic and anionic species are alternatively adsorbed on the sensor surface to create a multilayer thin film, as schematically reported in Fig. 4. Silica nanospheres or nanoparticles (SiO_2-NPs) can be included in the process to endow the film with high porosity and enhanced sensitivity. Specific functional compounds may be also infused into the coatings to provide specificity (Korposh et al., 2017; Rivero et al., 2019).

Other polymers are: polyvinyl alcohol (PVA) and polyimide (PI) (Ascorbe et al., 2017) due to their hydrophilic natures; hydrogels based on swelling/deswelling properties as function of pH; polystyrene (PS) and polydimethylsiloxane (PDMS) due to their affinity for organic compounds (Mensitieri et al., 2003) and others.

Metal oxide materials are also very important, based on their thermal stability, sensitivity, robustness and durability. When the target analyte interacts with the metal oxide, the electrical conductivity/dielectric constant of the latter changes (Pawar and Kale, 2019). Several metal oxide-based nanostructures and composites have been considered so far for LPGs, including titanium dioxide (TiO_2), tin dioxide (SnO_2), zinc oxide (ZnO), cuprous oxide (Cu_2O), tungsten trioxide (WO_3) and indium tin oxide (ITO).

Metal organic frameworks (MOFs) exhibit highly porous crystalline structures and are very flexible materials in terms of tunability and structural diversity (Kreno et al., 2012). Recently, novel 2D nanomaterials as graphene (Gr) and graphene oxide (GO) have become significant for chemical sensors, due to their physicochemical properties, including high specific surface area, electronic mobility and robustness (Hernaez et al., 2017).

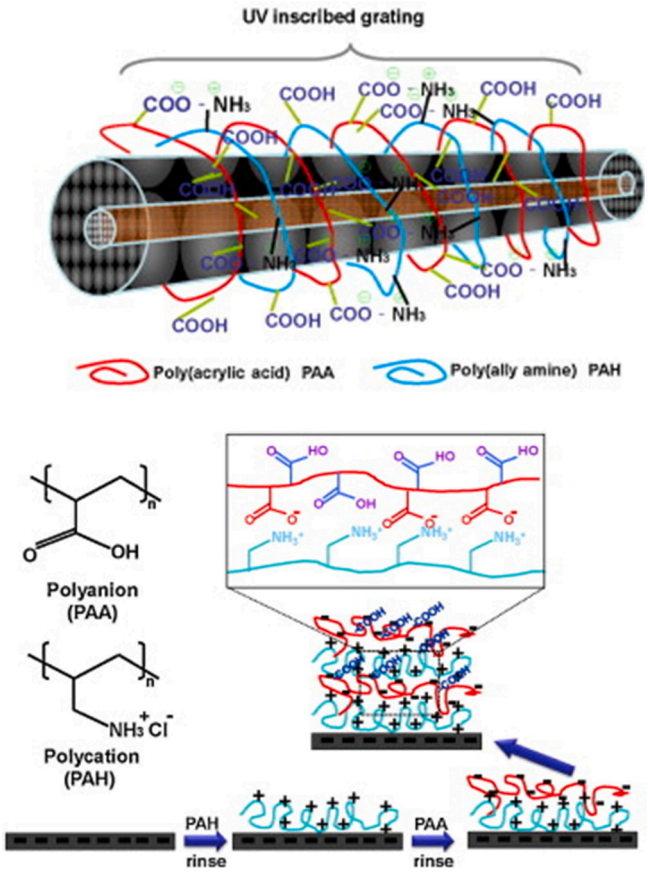

Fig. 4. Schematic picture of an LPG coated with PAH/PAA polyelectrolyte film. Adapted with permission from (Wang et al., 2013). © Elsevier.

Additional details regarding the nanomaterials for fiber optic chemical sensors can be found in the exhaustive reports from literature (Elosua et al., 2017; Pawar and Kale, 2019; Yin et al., 2018).

3. Results

This section describes the results obtained in the development of LPG-based chemical sensors. The works and related comments are mainly grouped based on the targets. For each work, the following information is reported: grating fabrication parameters and sensing configuration; sensitive materials and their properties; performance of the final sensor in terms of investigated range, limit of detection and sensitivity. The main parameters regarding sensor configuration and their performance are also summarized in Table 1 for the sake of comparison.

3.1. Relative humidity

The monitoring of relative humidity (RH) is crucial in different fields, such as industrial, medical, environmental monitoring, farming, food processing and so on. Different configurations of LPG transducers and sensitive materials have been employed for the purpose so far.

In (Venugopalan et al., 2008) the authors investigated an LPG written in single mode fiber by UV method with a period Λ of 300 μm, coated with a thick layer (~4 μm) of PVA due to its swelling properties with moisture. The sensor was tested in the range 33–97%RH and the intensity change of the resonance dip was monitored, obtaining a maximum change of about 2 dB. The sensitivity of the device was not constant in the mentioned range and increased at higher RH values, whereas a response time of about 80 s was recorded. Later, the same group also investigated different configurations of the transducer and sensitive material. Hence, in (Alwis et al., 2013a) the LPG (UV, 250 μm) was arranged in reflection configuration forming a Michelson interferometer (MI) to develop a single-ended probe, by cutting the fiber after the grating and coating a silver mirror onto the fiber tip. The device was tested in the range 20–85%RH and the dip wavelength of fringe interferences was monitored obtaining higher sensitivity in comparison to the previous work. Differently, in (Alwis et al., 2013b) they selected polyimide as hygroscopic material due to its linear swelling with humidity, whereas the LPG (UV, 330 μm) was similarly arranged in reflection configuration. In this case, a linear sensitivity of − 100 pm/RH % was obtained in the range 20–80%RH. Hysteresis was also evaluated and found to be negligible.

The group of the work (Viegas et al., 2009a) employed a sensitive multilayer of PAH/PSS, followed by PAH with SiO_2-NPs, with a thickness of a few hundreds of nm (around 300 nm). The atomic force microscopy (AFM) image of SiO_2-NPs surface is reported in Fig. 5(a). An LPG with 240 μm period was used as transducer. An exponential response of the resonance wavelength with humidity was found in the range 20–80%RH, while the temperature cross-sensitivity was linear. The authors also studied the effect on the sensitivity when changing the intermediate coating, as for example by using PDDA and PolyR-478 (Viegas et al., 2009b), and the comparative results are illustrated in Fig. 5(b). Based on such experience, the authors developed a sensor for the simultaneous measurement of temperature and RH based on an arc induced LPG (395 μm) coated with PDDA/PolyR and PAH/SiO_2-NPs, cascaded with a FBG (Viegas et al., 2011). The sensitivities to humidity were − 67.3 pm/%RH and − 451.8 pm/%RH, respectively, in the range 20–50%RH and 50–80%RH, whereas a response time of hundreds of ms was achieved.

On a different strand, the group of Cusano investigated LPG-based humidity sensors for high energy physics applications in (Berruti et al., 2014; Consales et al., 2014). An LPG (UV, 404 μm) was coated with a nanosized layer (~100 nm) of TiO_2 and tested in the range 0–75% RH showing an exponential response with a maximum sensitivity of − 1.4 nm/%RH at low humidity values (few %RH). A microscope picture of the LPG is reported in Fig. 6(a), whereas the spectra of the grating before and after deposition are compared in Fig. 6(b). The humidity response at different temperatures and after exposure to gamma radiation (up to 1 Mrad) was also evaluated to confirm its suitability for the specific application. The authors also investigated the behavior of an LPG coated with SnO_2 layer for the same purpose.

More recently, novel materials have been employed for the detection of relative humidity, as for example graphene oxide. In (Dissanayake et al., 2018) an UV induced LPG with $\Lambda = 400$ μm was coated with GO (~1.5 μm thick) and demonstrated a linear sensitivity of 0.15 dB/%RH in the range 60–95%. Differently, in (Tsai et al., 2021) a novel structure of LPG based on a periodic S-type photoresist grating was coated 1 μm GO. In this case, a sensitivity of 0.18 dB/%RH was achieved in the range 20–80%RH, when the fiber diameter was thinned down to 37 μm.

3.2. pH

Measurement of pH is also an important issue in environmental, chemical and clinical fields.

In (Corres et al., 2007a, 2007b), the authors investigated the possibility of measuring it using LPG-based sensors. They studied a coating configuration based on PAH/PAA and another where Prussian blue (PB) was added to PAH, with a thickness of about 400 nm. The results for PAH/PAA coated LPG are reported in Fig. 7. A linear sensitivity up to 28.3 nm/pH in the range 4–7 was obtained, by also designing the device to operate at mode transition region. Moreover, they found a tradeoff between response time (few minutes) and sensitivity, i.e., the introduction of PB into the polymeric matrix improves the first but decreases the latter.

PAH/PAA multilayer with similar thickness was also used in (Yang, 2014), in conjunction with a transducer based on cascaded LPG and FBG

Table 1
Details and performance of LPG-based chemical sensors.

LPG type and Λ	Nanomaterial	Target	Range (R); Lowest conc. (LC); LOD (L); Max. Sensitivity (S)	Ref.
UV 300 μm	PVA	RH	R: 33–97%	(Venugopalan et al., 2008)
UV 250 μm MI	PVA	RH	R: 20–85%	(Alwis et al., 2013a)
UV 330 μm	PI	RH	R: 20–80%; S: −100 pm/%RH	(Alwis et al., 2013b)
240 μm	PAH/PSS-PAH/SiO_2	RH	R: 20–80%	(Viegas et al., 2009a)
Arc 395 μm	PDDA/PolyR-PAH/SiO_2	RH	R: 20–80%; S: −451.8 pm/%RH	(Viegas et al., 2011)
UV 404 μm	TiO_2	RH	R: 0–75%; S: −140 pm/%RH	(Consales et al., 2014)
UV 400 μm	GO	RH	R: 60–95%; S: 0.15 dB/%RH	(Dissanayake et al., 2018)
Base S-type	GO	RH	R: 20–80%; S: 0.18 dB/%RH	(Tsai et al., 2021)
320 μm	PAH/PAA; PAH + PB/PAA	pH	R: 4–7; S: 28.3 nm/pH	(Corres et al., 2007b)
570 μm + FBG	PAH/PAA	pH	R: 4–10; S: 0.42 dB/pH	(Yang, 2014)
CO_2 330 μm	Hydrogel	pH	R: 2–12; S: 0.66 nm/pH	(Mishra et al., 2017)
UV 340 μm	sPS	Chloroform	R: 0–20 ppm; S: −0.85 nm/ppm	(Cusano et al., 2006b)
236 μm + RDS	PDMS	Xylene	L: 300 ppm	(Barnes et al., 2008)
236 μm + RDS	PDMS/PMOS	Xylene	L: 134 ppm	(Barnes et al., 2010)
UV 120–180 μm	PDMS	Toluene	L: 100 ppm	(Peshko et al., 2005)
UV 180 μm TAP	CA4	Benzene; Toluene	R: 0–70000 ppm; LC: 231 ppm	(Topliss et al., 2010)
UV 97 μm TAP	CA4	Toluene	R: 0–400 ppm; L: 41 pm	(Partridge et al., 2014)
UV 111 μm TAP	PAH/SiO_2 + CA4 or CA8	Acetone; Benzene;Chloroform; Toluene	R: 0–300000 ppm; L: 2211 (A), 3057 (B),4382 (C), 2743 (T) ppm	(Hromadka et al., 2017a)
UV 111 μm TAP	ZIF-8	Methanol	R: 1790–27900 ppm; L: 1454 ppm	(Hromadka et al., 2015)
UV 520 μm	Silk fibroin	Methanol	R: 0–205 ppm	(Konstantaki et al., 2020)
UV 250 μm TAP	–	Methanol	L: $1.3 \cdot 10^{-3}$% vol; S: 803 pm/% vol	(Dandapat et al., 2021)
UV 109 μm TAP	ZIF-8	Acetone; Ethanol	R: 0–700 ppm; L: 5.6–6.7 ppm	(Hromadka et al., 2018a)
Arc 900 μm	PDMS	Acetone	R: 0–17000 ppm; L: 910 ppm	(Rodríguez-Garciapiña et al., 2021)
Arc	Cu_2O	Ethanol	R: 0–30% vol; L: 1.63% vol	(Monteiro-Silva et al., 2018)
CO_2 520 μm	Zeolite	Isopropanol	R: 0–50 ppm; LC: 5.5 ppm	(Zhang et al., 2009)
CO_2 330 μm	PAM gel + tyrosinase	Catechol	R: 0–800 μM; L: 6.8 μM; S: 9 pm/μM	(Mishra and Chiang, 2020)
CO_2 480 μm	SAN/cryptophane-A	Methane	R: 0–3.5% vol; L: 0.2% vol; S: 0.375 nm/%	(Yang et al., 2011)
CO_2 520 μm	PC/cryptophane-A	Methane	R: 0–3.5% vol; L: 0.2% vol; S: 2.5 nm/%	(Yang et al., 2015)
CO_2 480 μm in PCF	PAA-CNTs/PAH	Methane	R: 0–3.5% vol; L: 0.18% vol; S: 1.078 nm/%	(J. Yang et al., 2017b)
CO_2 600 μm SPR	Ag + Graphene	Methane	R: 0–3.5% vol; S: 0.344 nm/%	(Wei et al., 2016)
UV 360 μm	aPS	Butane	R: 0–1.0% vol; S: −2.2 nm/% vol	(Esposito et al., 2018d)
UV 475 μm + FBG	WO_3	Hydrogen	R: 0–4%	(Caucheteur et al., 2008)
CO_2 520 μm	SCZY	Hydrogen	R: 0–60%	(Tang et al., 2009)
CO_2 520 μm	ZSM-5	Ammonia	–	(Tang et al., 2011)
UV 100 μm TAP	PDDA/SiO_2 + TSPP	Ammonia	R: 0.1–10 ppm; L: 0.14 ppm	(Korposh et al., 2012a)
UV 100 μm TAP	PAH/PAA	Ammonia	R: 0–350 ppm; L: 10.7 ppm	(Wang et al., 2013)
UV 100 μm TAP	PDDA/TSPP	Ammonia	R: 0–350 ppm; L: 0.67 ppm	(Wang et al., 2016)
CO_2 430 μm in PCF	–	Ammonia	R: 0–165 ppm; S: 17.3 nW/ppm	(Zheng et al., 2016)
2x CO_2 320 MZI	Graphene	Ammonia	R: 10–180 ppm; S: 3 pm/ppm	(Hao and Chiang, 2017)
CO_2	GO/CA	Ammonia	R: 0–8 ppm; S: 98.3 pm/ppm	(Xu et al., 2021)
450 μm	aPS	Carbon dioxide	R: 0–100%; S: 1.23 pm/%	(Melo et al., 2014)
notched 600 μm	TEPA	Carbon dioxide	R: 6–15%; S: −0.089 dB/%	(Wu and Chiang, 2015)
notched 600 μm	ZnO-NPs	Carbon dioxide	R: 3–15%; S: 0.0513 dB/%	(Wu et al., 2016)
UV 109 μm TAP	HKUST-1	Carbon dioxide	R: 2000–40000 ppm; L: 401 ppm	(Hromadka et al., 2018b)
CO_2 570 μm	GO	Nitric oxide	R: 0–400 ppm; S: −63.6 pm/ppm	(Xu et al., 2019)
notched 650 μm	WO_3	Nitric oxide	LC: 500 ppm	(Wen et al., 2020)
560 μm	$MoS_2/C_6H_7O_8$	Hydrogen sulfide	R: 0–70 ppm; L: −0.5 ppm; S: 10.5 pm/ppm	(Qin et al., 2018)
UV 110 μm TAP	Hb	Dissolved oxygen	–	(Partridge et al., 2016)
LPG	PMO	Lead ions	R: 0.1–1.0 ppm; L: 20 ppb	(Du et al., 2010)
Arc 650 μm	PDDA/PSS-PDDA/Au-NPs	Mercury ions	R: 0.5–10 ppm	(Tan et al., 2018)
CO_2 680 μm	GO	Nickel ions	R: $1–10^7$ ppb; L: 2.5 ppb; S: $5.1 \cdot 10^{-4}$ nm/ppb	(Wang et al., 2020a)
400 μm in μfiber	–	Chromium ions	R: 0.195–200 ng/mL; L: 0.219 ng/mL	(T. Huang et al., 2021b)
CO_2 500 μm SPR	Au/GSH	Arsenic ions	R: 0.02–2.0 ppb; L: 0.04 ppb	(C. Huang et al., 2021a)
2x Arc 520 μm MZI	–	Marine salinity	R: 0–150 g/L; S: −5 pm/(g/L)	(Possetti et al., 2009)
CO_2 247 μm	CHI/PAA	Marine salinity	R: 0.1–0.8 M; S: −36.2 nm/M	(F. Yang et al., 2017a)
CO_2 247 μm	qP4VP hydrogel	Marine salinity	R: 0.4–0.8 M; S: 7 nm/M	(Yang et al., 2019)
LPG	GO	SCC	S: 0.0587 dB/(mg/L); L: 0.17 mg/kg	(Li et al., 2021)
UV 100 μm TAP	PAH/SiO_2	Mellitic acid	LC: 1 nM	(Korposh et al., 2012b)
UV 500 μm in MMF	–	Methylene blue	LC: 10 nmol/L	(Thomas Lee et al., 2003)
Arc 650 μm	ITO	Methylene blue	R: 0.001–1 mM	(Okazaki et al., 2020)

with corroded cladding interrogated in reflection. A maximum sensitivity of 0.42 dB/pH was found in the range 4–10.

Finally, a wide range of pH was investigated in (Mishra et al., 2017), where an LPG fabricated by CO_2 laser with a period of 330 μm was coated with a hydrogel material having a thickness of about 530 nm. The sensitivity was about 0.66 nm/pH in the range 2–12 and the response time was less than 2 s.

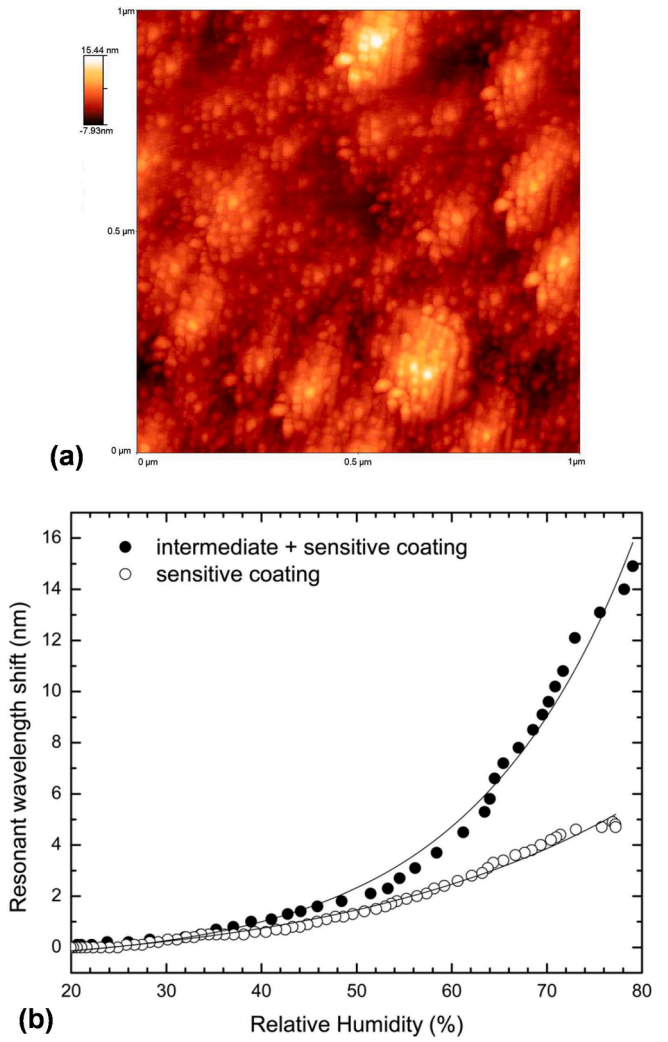

Fig. 5. (a) AFM image of SiO_2-NPs coating; (b) Comparison of the response to RH of two LPGs coated with PAH/SiO_2-NPs and PDDA/PolyR-PAH/SiO_2-NPs. Adapted from (Viegas et al., 2009b). Under a Creative Commons license.

3.3. Volatile organic compounds

The monitoring of VOCs is quite important for the global environment and human beings, due to their toxicity, harmful and pollutant nature.

The works reported in (Allsop et al., 2001; Falate et al., 2005) were probably among the first ones regarding LPG-based sensors for the detection of VOCs, after these many other examples have followed. Specifically, in (Allsop et al., 2001) the detection of 0.04% vol (corresponding to 400 ppm) of xylene (C_8H_{10}) in heptane solution was demonstrated. Whereas, the authors of (Falate et al., 2005) showed the detection of hydrocarbons in fuel (i.e., turpentine, naphtha, paint thinner, anhydrous alcohol), in air (butane, propane) and in water (gasoline). In the mentioned cases, the working principle was based on the RI change due to the presence of the analyte, without selectivity.

Moreover, the use of PDMS as sensitive coating was also investigated soon after. In (Peshko et al., 2005), the authors used it to coat an LPG (period shorter than 200 µm) for the detection of toluene (C_7H_8) achieving a LOD of 100 ppm. Another example is the work in (Barnes et al., 2008), where the use of functionalized PDMS coating of 20 µm, etched LPG (Λ = 236 µm) and interrogation based on fiber-loop ring-down spectroscopy (RDS) permitted the detection of xylene vapors with a LOD of 300 pm. The same authors also employed a coating based on PDMS/polymethyl-octylsiloxane (PDMS/PMOS) and phase-shift cavity

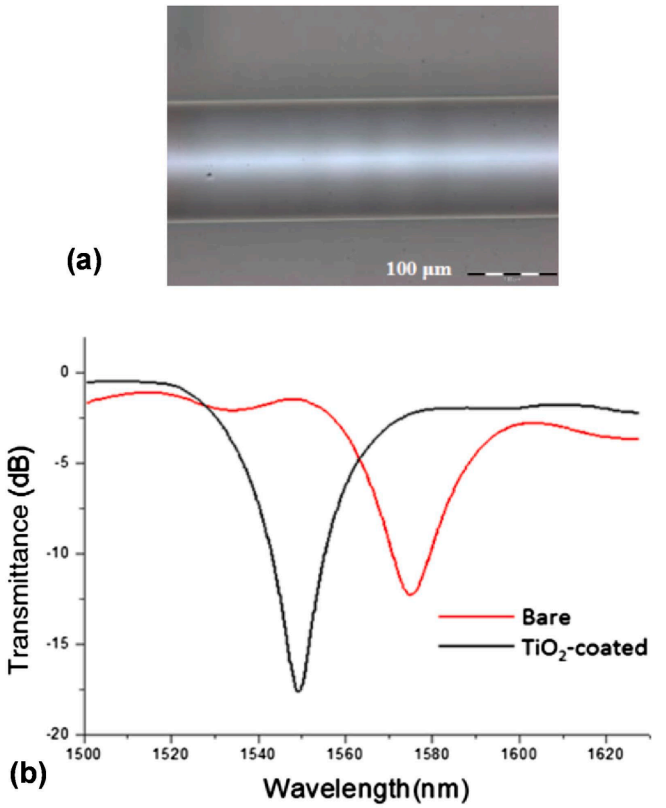

Fig. 6. LPG coated with TiO_2 for RH measurement: (a) Microscope image of TiO_2 coating onto the fiber; (b) Transmission spectra of bare and coated LPG. Adapted with permission from (Consales et al., 2014). © The Optical Society.

RDS interrogation, improving the LOD for xylene down to 134 ppm and for the detection of other hydrocarbons (Barnes et al., 2010).

Following the discovery of mode transition phenomenon, the detection of chloroform ($CHCl_3$) in water was demonstrated in (Cusano et al., 2006b; Pilla et al., 2005) by using an LPG coated with delta form of syndiotactic polystyrene (sPS). The LPG was UV written with a period of 340 µm and the thickness of sPS layer was selected equal to 260 nm for MT. A sensitivity of − 0.85 nm/ppm was obtained in the range 0–20 ppm, with reversible behavior.

Differently, TAP LPGs have been also widely investigated regarding the detection of VOCs. In (Topliss et al., 2010) the authors employed an LPG (Λ = 180 µm) coated with a calixarene (CA), calix-4-resorcarene (CA4), with optimized thickness of about 190 nm to benefit of mode transition as well. The evolution of the transmission spectrum as a function of the CA thickness is reported in Fig. 8, highlighting MT and dual resonance TAP operation. The detection of toluene and benzene (C_6H_6) vapors in the range 0–70000 ppm by volume was performed. Selectivity was investigated using hexane and cyclohexane. The authors also investigated the detection of toluene in water using a similar configuration of transducer and coating (Partridge et al., 2014): they found a LOD of 41 ppm in the range 0–400 pm by mass, selectivity was also confirmed by using ethanol. In (Hromadka et al., 2017a) a TAP LPG, modified with a 250 nm thin mesoporous coating of PAH/SiO_2-NPs infused with CA4 or CA8, was exposed to acetone (C_3H_6O), benzene, chloroform and toluene vapors in the range 0–300000 ppm. The sensor with CA4 exhibited a stronger response than with CA8, moreover the highest signal was observed for acetone and the lowest for chloroform, whereas the response time was shorter than 1 min. The LODs were 2211 ppm for acetone, 3057 ppm for benzene, 4382 ppm for chloroform and 2743 ppm for toluene. The same authors also developed a multi-parameter system for the monitoring of indoor air quality in (Hromadka et al., 2017b), where an array of three LPGs with different

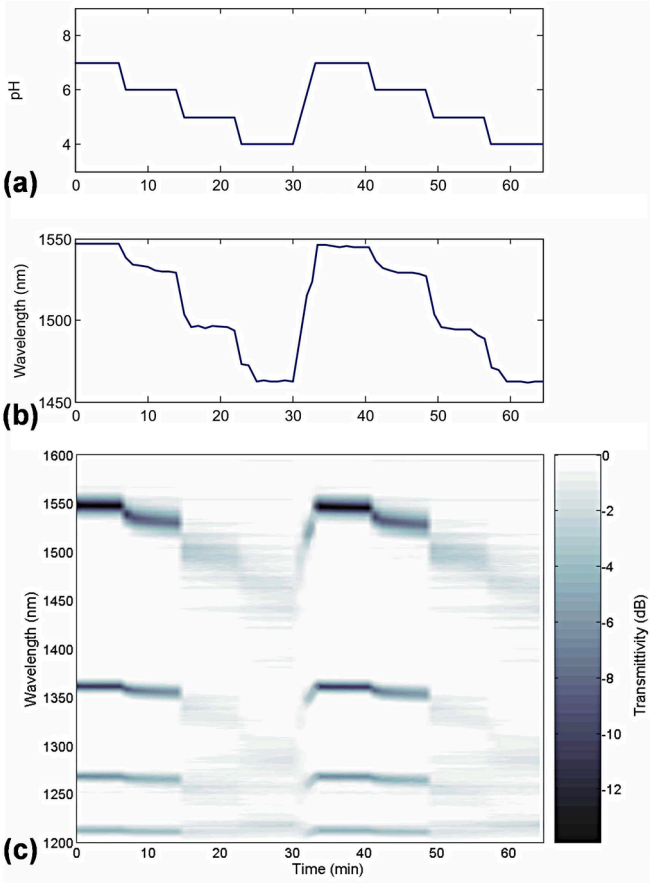

Fig. 7. LPG coated with PAH/PAA for the measurement of pH: (a) Solution pH; (b) Wavelength shift of the highest order cladding mode; (c) Evolution of the transmission spectrum during test at different pH values. Adapted with permission from (Corres et al., 2007a). © The Optical Society.

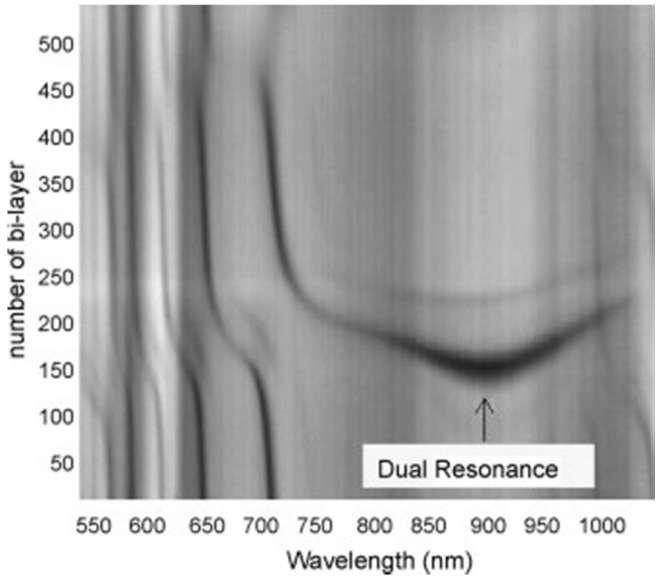

Fig. 8. LPG coated with calixarene for the detection of toluene: evolution of the transmission spectrum as a function of CA thickness (number of bi-layers). Dark trails illustrate the resonance wavelengths of the attenuation bands. Adapted with permission from (Topliss et al., 2010). © Elsevier.

coatings was used for the measurement of temperature, RH and VOCs (acetone, benzene, chloroform, toluene). Very recently, the authors of (Dandapat et al., 2021) reported the detection of methanol (CH_4O) and water in biofuel with a TAP LPG (period 250 μm). Sensitivities within 750–800 pm/% vol and LOD of about $1.3 \cdot 10^{-3}$% vol were achieved, even if without a selective coating.

The use of metal organic framework materials is also worth to be highlighted in this context. In (Hromadka et al., 2015), a TAP LPG was coated with a zeolitic imidazolate framework ZIF-8 film of 350 nm, whose scanning electron microscopy (SEM) images are reported in Fig. 9. The detection of methanol concentrations within 1790–27900 ppm was performed achieving a LOD of 1454 ppm. The selectivity was tested by using ethanol, isopropanol and acetone. Whereas in (Hromadka et al., 2018a), similar configuration of transducer and ZIF-8 coating with a few data analysis techniques was considered. The detection of acetone and ethanol (C_2H_6O) was performed in the range 0–700 ppm with LODs of 6.7 and 5.6 ppm, respectively. Very recently, the real-time adsorption/desorption of VOCs in MOFs has been studied in (Wu et al., 2021) by an LPG.

Several other materials were also employed for the detection of different VOCs. Zeolite film of about 10 μm was used to coat an LPG (CO_2, 520 μm) for the detection of organic vapors, i.e., isopropanol (C_3H_8O) and toluene, achieving ppm and sub-ppm LODs, respectively (Zhang et al., 2009). The response time to isopropanol was 2 min while it took much longer for toluene. In (Konstantaki et al., 2012), zinc oxide nanorods (ZnO-NRs) with thickness of a few μm were used to coat an LPG for the detection of ethanol vapors. In (Monteiro-Silva et al., 2018) an arc discharge induced LPG was coated with Cu_2O with thickness of

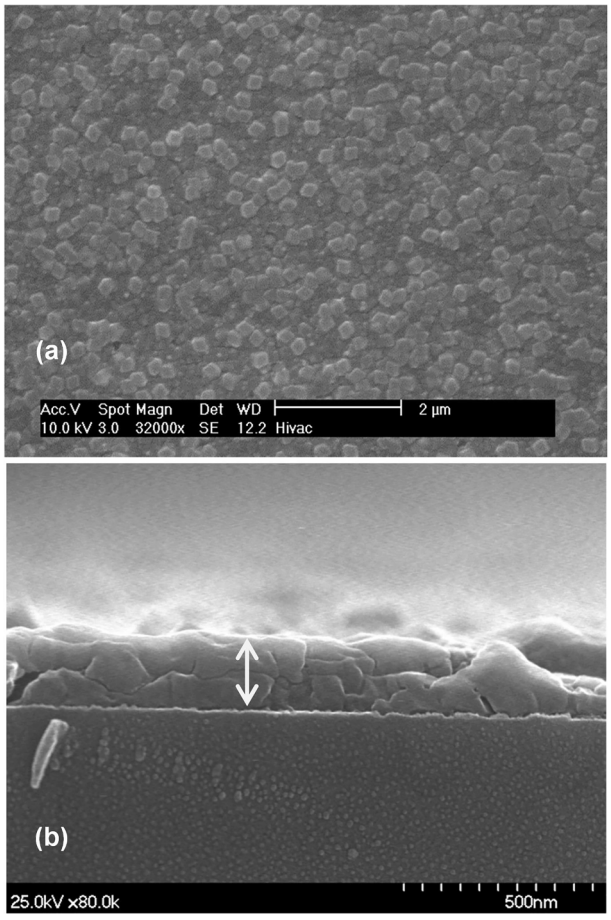

Fig. 9. SEM images of ZIF-8 film on glass substrate: (a) top and (b) cross section view. Adapted from (Hromadka et al., 2015). Under a Creative Commons license.

about 50 nm, for the detection of ethanol in gasoline mixtures: a LOD of 1.63% vol was obtained in the range 0–30% vol. Silk fibroin with a thickness of 400 nm was used as sensitive coating for the detection of methanol vapor in the range 0–205 ppm (Konstantaki et al., 2020). A phenolic-compounds sensor based on LPG coated with an enzyme-entrapped poly-acrylamide (PAM) gel was investigated by the authors of (Mishra and Chiang, 2020). The used enzyme is tyrosinase and thickness of the gel is around 900 nm. The sensor was tested for the detection of catechol ($C_6H_6O_2$) concentrations within 0–800 μM in aqueous solution, achieving a LOD of 6.8 μM and a sensitivity of 9 pm/μM. The selectivity was also tested by using m-cresol, 4-chlorophenol and phenol. Whereas, in (Rodríguez-Garciapiña et al., 2021), the authors investigated different configurations of arc LPGs, i.e., single and paired forming a Mach-Zehnder interferometer (MZI), coated with PDMS and applied principal component analysis (PCA). For example, in the case of LPG with 900 μm period, the LOD for acetone detection is 910 ppm whereas the range investigated is 0–17000 ppm.

Methane (CH_4) gas sensing has been also widely investigated due to its flammability. The authors of (Yang et al., 2011) employed a styrene-acrylonitrile (SAN) film incorporating cryptophane-A to coat an LPG (CO_2, 480 μm), with a thickness of about 500 nm. The detection of methane in the range 0–3.5% vol with a LOD of 0.2% vol, sensitivity of 0.375 nm/% and response time of 50 s was achieved. Almost no interference from dry air, O_2, CO, CO_2 and H_2 was found. The same authors (Yang et al., 2015) investigated a coating of polycarbonate (PC)/cryptophane-A with optimized thickness of 530 nm to induce MT. The sensor presented high RI sensitivity of − 3500 nm/RIU, resulting in a sensitivity of 2.5 nm/% to methane concentration. They also investigated a different transducer in (J. Yang et al., 2017b), where they considered an LPG written in a PCF and coated the inner air holes with cryptophane-A absorbed on a PAA-carbon nanotubes/PAH (PAA-CNTs/PAH) film with a thickness of 210 nm. Moreover, the authors of (Wei et al., 2016) developed a planer device with an LPG covered with Ag and graphene, based on SPR phenomenon. Methane detection in the range 0–3.5% was performed with a sensitivity of 0.344 nm/%.

Finally, the detection of butane (C_4H_{10}) gas using an LPG (UV, 360 μm) coated with atactic polystyrene (aPS) in reflection configuration was reported in (Esposito et al., 2018d). The thickness of aPS was designed equal to about 350 nm to have mode transition phenomenon. The sensor was tested in the range 0–1.0% vol showing a maximum sensitivity of − 2.2 nm/% vol at lower concentrations, as reported in Fig. 10. Moreover, the sensor was employed for the detection of liquefied petroleum gas in a railway tunnel in (Esposito et al., 2018c).

3.4. Environmental and hazardous gases

In this context, the detection of hydrogen (H_2) was one of the first investigated targets due to its explosivity. For example, in (Caucheteur et al., 2008) a WO_3 film doped with Pt on its surface was used to coat an hybrid configuration made of UV-written LPG and FBG. The working principle is based on temperature increase due to exothermic reaction of H_2 on the catalytic film. The response to hydrogen was investigated in the range 0–4% vol down to a temperature of − 50 °C and in both dry and moist environments. Another example is the work in (Tang et al., 2009), where an LPG (CO_2, 520 μm) coated with a proton conducting perovskite oxide thin film (SCZY) of about 500 nm was investigated for the detection of hydrogen at high temperatures. The device was tested in the range 0–60% and up to 500 °C, whereas selectivity was confirmed by exposing the sensor to CO, CH_4, CO_2, H_2O and H_2S. The same authors also investigated the possibility to protect the SCZY layer from fine ash mineral particles and large contaminating molecules by using a silicalite layer in (Jiang et al., 2013) for in-situ monitoring. Finally, the possibility to use a TAP LPG coated with a palladium (Pd) layer for hydrogen detection was numerically investigated in (Basumallick et al., 2016).

Ammonia (NH_3) is one of the most widely investigated species by LPG-based sensing platforms, due to its toxicity and flammability. For example, in (Tang et al., 2011) a zeolite ZSM-5 film of 3–4 μm was used to coat a CO_2 laser written LPG (period 520 μm). The authors studied the temperature influence (up to 200–300 °C) on the sensing performance and selectivity by exposing the device to H_2, CO_2, H_2S and H_2O. Differently, in (Korposh et al., 2012a) the authors employed a mesoporous coating of PDDA/SiO_2-NPs (thickness of 450 nm) infused with tetrakis-(4-sulfophenyl)porphine (TSPP) onto a TAP LPG for ammonia sensing in aqueous solution. The detection in the range 0.1–10 ppm, a LOD of 0.14 ppm and response time of 100 s were achieved. The same authors investigated the detection of ammonia gas in (Wang et al., 2013) by coating a similar LPG with a multilayer of PAA/PAH (thickness around 200 nm). A LOD of 10.7 ppm was obtained in the range 0–350 ppm. The selectivity was also investigated using several amine and non-amine compounds, such as triethylamine, trimethylamine, pyridine, ethanol and methanol. After few years, they also investigated the coating of PDDA with TSPP for ammonia gas detection improving the LOD down to 0.67 ppm in (Wang et al., 2016). Related spectra and response of the device are reported in Fig. 11(a) and 11(b), respectively. Also in this case, selectivity was verified by using chloroform, acetone, methanol, ethanol, acetic acid, benzene and toluene. Moreover, an unconventional PCF-based spectroscopic absorption sensing platform assisted by an LPG was presented in (Zheng et al., 2016). The device is operated in reflection configuration and coupled with an Er-doped fiber ring laser. A sensitivity of 17.3 nW/ppm was found in the range 0–165 ppm of gaseous ammonia. The device presented selectivity, which was confirmed using methanol and methane. Recently, graphene and GO have been also investigated as sensitive coatings for ammonia gas. For example, in (Hao and Chiang, 2017) two LPGs (written by CO_2 with periods of 320 μm) forming a MZI were employed. The device was

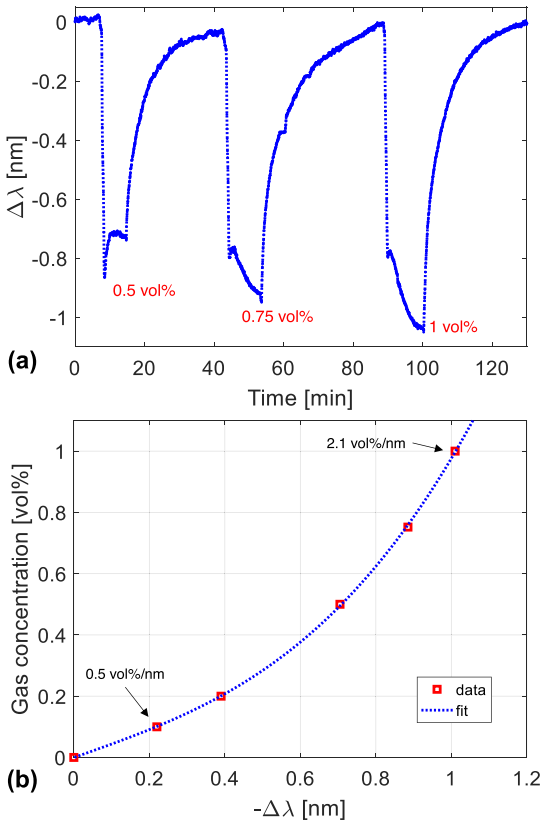

Fig. 10. LPG coated with aPS for the detection of butane gas: (a) Response of the sensor to different butane concentrations as a function of the time; (b) Relationship between wavelength shift and butane concentration. Adapted from (Esposito et al., 2018c). Under a Creative Commons license.

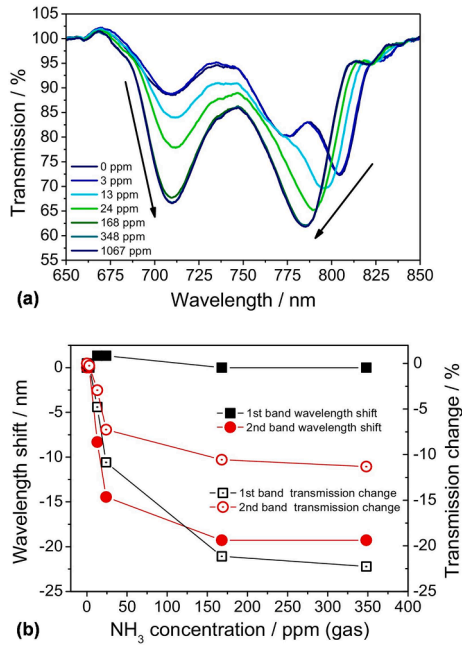

Fig. 11. LPG coated with PDDA/TSPP film exposed to ammonia gas: (a) Transmission spectra; (b) Response of the sensor. Adapted with permission from (Wang et al., 2016). © Elsevier.

coated with graphene and exhibited a sensitivity of 3 pm/ppm in the range 10–180 ppm. Whereas, in (Xu et al., 2021) an LPG was coated with a graphene oxide/cellulose acetate (GO/CA) composite coating. A sensitivity of − 98.3 pm/ppm was obtained in the range 0–8 ppm, with a response time of 32 s. Selectivity was confirmed by exposing the device to N_2 and SO_2.

Different LPG configurations have been employed also for the detection of carbon dioxide (CO_2) due to toxicity and pollutant nature. In (Melo et al., 2014) an LPG was coated with a thin layer of aPS, where the grating had a period of 450 μm and the thickness of aPS was designed to be equal to 365 nm for MT. A sensitivity of 1.23 pm/% was achieved with the possibility to distinguish between CO_2 and N_2. Differently, in (Wu and Chiang, 2015), an unconventional notched LPG fabricated through inductively coupled plasma (ICP) etching with a period of 600 μm was coated with a layer of tetraethylenepentamine (TEPA)-modified adsorbent. A sensitivity of − 0.089 dB/% in the range 6–15% of CO_2 was obtained. The same authors used a similar transducer coated with ZnO-NPs and obtained similar performance in (Wu et al., 2016). Moreover, the authors of (Hromadka et al., 2018b) employed a Cu-based MOF, HKUST-1, to coat a TAP LPG ($\Lambda = 109$ μm). The thickness of the film was of tens of nm (around 55 nm). The sensor responded to CO_2 concentrations in the range of 2000–40000 ppm and the LOD of 401 ppm was obtained.

The detection of nitric oxide (NO) has been also a matter of study. In (Xu et al., 2019) the authors developed a device based on a GO layer (around 50 nm) onto an LPG written by CO_2 with a period of 570 μm. The sensor was investigated in the range 0–400 ppm and presented a maximum sensitivity of − 63.6 pm/ppm up to about 80 ppm. The response time was several minutes and selectivity was confirmed by exposing the sensor to NH_3 and SO_2. A not fully reversibility behavior was observed. More recently, notched LPG was employed for the detection of 500 ppm of NO using a coating of WO_3 in (Wen et al., 2020).

Due to its poisonous nature, the detection of hydrogen sulfide (H_2S) was also performed, for example, in (Qin et al., 2018). For the purpose, an LPG with a period of 560 μm was coated with a molybdenum sulfide/citric acid ($MoS_2/C_6H_7O_8$) composite membrane. A low LOD of 0.5 ppm was obtained and a sensitivity of − 10.5 pm/ppm in the range 0–70 ppm. Response time of 89 s was measured and a good selectivity by exposing the device to several gases in the air (N_2, CO_2, O_2 and Ar).

Finally, the authors of (Partridge et al., 2016) preliminarily investigated the possibility to monitor dissolved oxygen (DO) by coating an LPG with hemoglobin (Hb). For the purpose, the sensitivity to the ratio of dissolved carbon dioxide to dissolved oxygen is demonstrated via the conversion of carboxyhemoglobin to oxyhemoglobin on the sensor surface.

3.5. Heavy metal ions

Heavy metal ions are widely employed by the industries for various applications, being released in natural resources of water and representing a risk for both and aquatic life.

One of the first reports about this topic can be found in (Du et al., 2010) where an LPG was coated with a periodic mesoporous organosilica (PMO) film, with thickness of about 2 μm, for the detection of lead ions (Pb^{2+}). The range 0.1–1.0 ppm was investigated and a LOD of 20 ppb was achieved.

In (Tan et al., 2018) an arc induced LPG (650 μm) was coated with a multilayer of PDDA/PSS and Au-NPs for the detection of mercury ion (Hg^{2+}) concentrations in the range 0.5–10 ppm.

Whereas, in (Wang et al., 2020a) the authors used an LPG fabricated by CO_2 laser with a period of 680 μm and coated with a 216 nm GO layer for the detection of nickel Ni^{2+} in water. The range of concentrations 1–10^7 ppb was investigated, obtaining a sensitivity of $5.1 \cdot 10^{-4}$ nm/ppb and a LOD of 2.5 ppb.

Very recently, a microfiber LPG was integrated with a lateral flow immunoassay biosensor and tested for the detection of chromium ions (Cr^{3+}) in (T. Huang et al., 2021b). The fiber diameter was 11 μm whereas the grating period was 400 μm and the working principle was based on the refractive index change induced by localized plasmonic heating of antibody-conjugated Au-NPs through a laser. The range 0.195–200 ng/mL was investigated and a LOD of 0.219 ng/mL was achieved. Selectivity test using several other metal ions was also performed.

Finally, the detection of arsenic ions (As^{3+}) was demonstrated in (C. Huang et al., 2021a). An LPG (CO_2, 500 μm) was coated with an Au layer and functionalized with glutathione (GSH). The sensitivity was further improved by using a sandwich structure with GSH-modified Au-NPs. The range investigated was 0.02–2.0 ppb with a LOD of 0.04 ppb. Selectivity was also verified by using other metal ions.

3.6. Corrosion monitoring

Corrosion monitoring of steel and reinforced concrete structures is of vital importance for the safety and maintenance of civil infrastructures.

In this framework, the authors of (Huang et al., 2013) studied an LPG coated with Fe- and SiO_2-NPs in a polyurethane (PU) matrix (thickness of 2.5 μm) by monitoring the corrosion rate of Fe-NPs in a corrosive environment. The envisaged application of such device is the deployment in proximity of a steel bar/member and subsequent correlation to monitor the corrosion rate of steel. Temperature and pH cross sensitivities were also evaluated. Proof-of-concept test was performed in 3.5% wt NaCl solution for one month. Based on such experience, the authors applied their sensor for the monitoring of mass loss rate of steel bars in (Huang et al., 2015).

In (Chen et al., 2016), an LPG (induced by CO_2 method with 387 μm period) was coated with micrometric thick layers of Ag and Fe-C for corrosion monitoring of low carbon steel in 3.5% wt NaCl solution. The resonance wavelength shift of the sensor was correlated with the steel mass loss, obtaining a sensitivity of 0.0423 nm/% up to 80% Fe-C mass loss and 0.576 nm/% in the range 80–95%. The tradeoff between sensitivity and service life of the sensor was also evaluated. The authors further optimized the coating properties in (Chen et al., 2017) by considering 0.8–1.2 μm thick Ag layers and 8–20 μm Fe-C layers, whose morphologies taken by SEM are illustrated in Fig. 12. Moreover, they

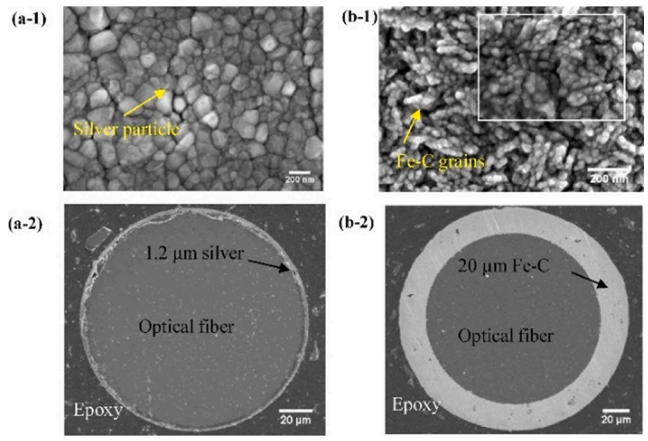

Fig. 12. SEM images of surface (1) and cross sectional (2) morphologies of (a) Ag film and (b) Fe-C coating deposited onto an optical fiber for corrosion monitoring. Adapted with permission from (Chen et al., 2017). © Elsevier.

applied the sensors for the monitoring of corrosion-induced mass loss of steel bar in NaCl solution and in mortar cylinder (Tang et al., 2018).

The authors of (Coelho et al., 2018) employed arc induced LPGs (399 μm) coated with Fe thin films (thicknesses of 10–40 nm) and exposed them to oxidation in air and water at different concentrations of NaCl, to monitor the formation of iron oxides and hydroxides. In the same work, the sensing characterization of an LPG coated with hematite (Fe_2O_3) was also performed obtaining a sensitivity of − 1611 nm/RIU for an external refractive index in the range 1.42–1.46.

Recently, in (Guo et al., 2020) a Fe-C coated graphene/silver nanowires (Gr/Ag-NWs)-based LPG was tested in 3.5% wt NaCl solution for mass loss measurement under different strain levels and a correlation was provided. The thickness of Ag-NWs layer was 30 nm whereas that of Fe-C was 30 μm.

3.7. Marine salinity

The salinity in marine environment is an important parameter for the study of marine biology, oceanic currents and global climate change. The marine organisms and submarine activities are strongly influenced by the salinity in the marine environment and thus its measurement is vital.

In (Possetti et al., 2009), the authors employed two arc induced LPGs with period of 520 μm forming a MZI for salinity measurement in water solution. Two inorganic and one organic salts (NaCl, KCl, NaCOOH) were considered by using concentrations in the range 0–150 g/L. The working principle is based on the change of refractive index due to the presence of salts and an average sensitivity of − 5 pm/(g/L) was obtained. Temperature cross-sensitivity effect was also highlighted to be critical.

The authors of (F. Yang et al., 2017a) studied the integration of ionic-strength-responsive chitosan (CHI)/PAA (CHI/PAA) multilayers (average thickness of 3.3 μm) with a CO_2 written LPG having a period of 247 μm. The device was exposed to NaCl solutions in range 0.1–0.8 M at pH 7.5, including those of marine seawater and salt lakes. The device exhibited red shift with salinity in range 0.1–0.4 M, whereas a blue shift was observed in the range 0.5–0.8 M with a maximum sensitivity of − 36.2 nm/M, as reported in Fig. 13. The authors studied the swelling/deswelling mechanisms of the coating and found a dependence of the response upon the pH values at which the deposition and salinity measurement take place. Later, the same group integrated the LPG with micron scale overlays of partially quaternized poly(4-vinylpyridine) (qP4VP) hydrogel (Yang et al., 2019). The range of salinity 0.4–0.8 M was investigated obtaining a sensitivity of 7 nm/M, a response time shorter than 5 s and no response to varying pH around 8.1 of marine environment.

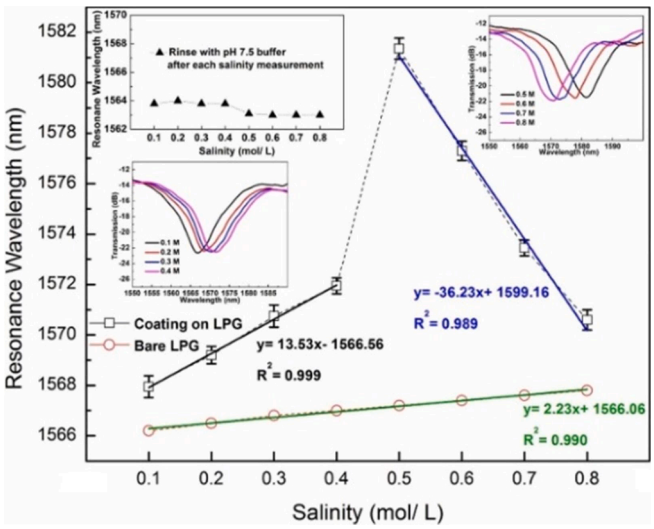

Fig. 13. Response to salinity concentrations of the LPG coated with CHI/PAA and bare LPG. The insets illustrate the spectra of the coated LPG during the characterization. Adapted with permission from (F. Yang et al., 2017a). © Elsevier.

3.8. Food quality assessment and other compounds

LPG sensors have been also investigated for the monitoring of food quality.

In particular, the authors of (Korposh et al., 2014) employed a TAP LPG (100 μm) coated with a 450 nm PAH/SiO_2-NPs film for the identification and quality assessment of different beverages, including: red and white wines, brandy and Japanese beverages. Fig. 14(a) illustrates the spectra of the LPG when immersed in the different beverages at fixed alcohol concentration, whereas Fig. 14(b) reports its response to different concentrations of ethanol. The results were compared with gas chromatography-mass spectroscopy to evaluate the volatile organic compounds contributing to the flavors of red wines. They employed PCA for data analysis and the possibility to detect high concentrations of compounds in wine (1–1000 mg/L) using few μL samples was demonstrated. Moreover, the method was adjusted for the quantification of selected compounds and the acetic acid was targeted.

Another example is the work in (Coelho et al., 2015), where the authors explored the possibility to detect the thermal deterioration of extra virgin olive oil, using an LPG (arc induced, $\Lambda = 396$ μm) coated with a TiO_2 film with thickness of 30 nm. The bulk RI sensitivity of the device is about − 800 nm/RIU in the range 1.46–1.48. The working principle of the device is based on the measurement of the refractive index change of oil due to temperature.

Very recently, the detection of sodium copper chlorophyllin (SCC), a porphyrin compound used as food colorant, was performed by using an LPG coated with GO and an enhanced photothermal signal detection method, resulting in a sensitivity of 0.0587 dB/(mg/L) and a LOD of 0.17 mg/kg (Li et al., 2021).

Other compounds were also considered as targets of chemical sensing based on LPGs. For example, the detection of methylene blue (MB) was performed in (Thomas Lee et al., 2003) which is among the first reports regarding LPG-based chemical sensors. The authors UV induced a grating with a period of 500 μm in a plastic MMF. They found a linear relationship between logarithm of the concentration and power associated to core mode (or cladding modes) and the lowest concentration of MB which could be detected was 10 nmol/L. Finally, in (Korposh et al., 2012b), a TAP LPG with PAH/SiO_2-NPs coatings (thicknesses around 200–600 nm) was used for the detection of several

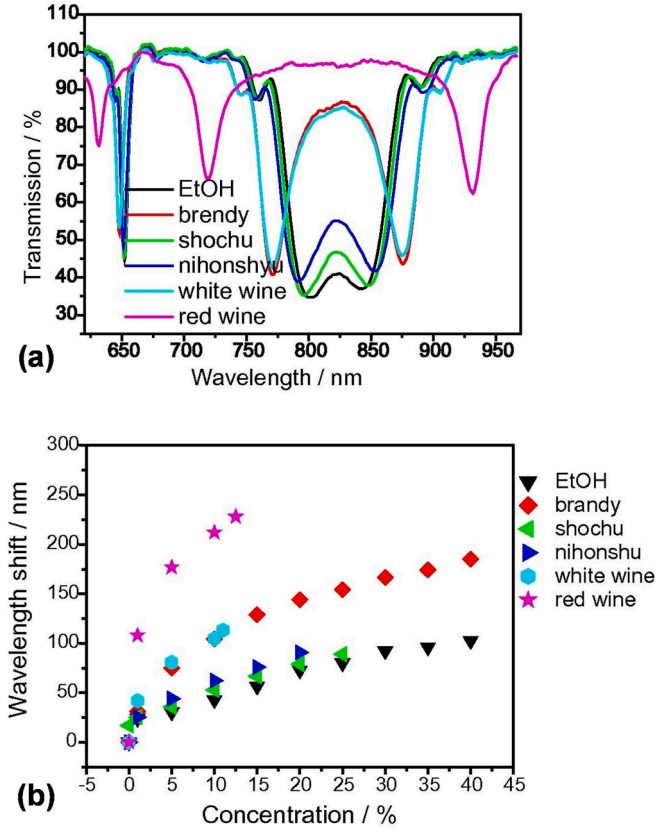

Fig. 14. LPG coated with PAH/SiO_2-NPs for beverage assessment: (a) Transmission spectra when immersed in different beverages (alcohol concentration of 10%); (b) Response as a function of ethanol concentration in different beverages. Adapted from (Korposh et al., 2014). Under a Creative Commons license.

aromatic carboxylic acids (ACA) by exploiting the acid-base interaction between their acid group and amino group of PAH. The lowest detectable concentration of 1 nM was achieved for mellitic acid (MA), moreover the response of the LPG was validated by quartz crystal microbalance and silicon wafer used in reflectometric interference spectroscopy.

3.9. Opto-electrochemical measurements

New multi-domain sensing approaches are being considered nowadays, as for example the employment of an optical sensor to enhance the amount of data collected during electrochemical analysis.

In this context, in (Janczuk-Richter et al., 2019) a TAP LPG with 248 μm period was coated with an electrically conductive film of ITO with thickness of about 75 nm. Refractometric sensitivity can reach up to − 5000 nm/RIU in the range 1.36–1.39. Here, ITO material has a twofold role: i) enhances the sensitivity of the LPG; ii) is the working electrode of the electrochemical setup reported in Fig. 15(a). It was found that the optical response of the LPG is highly dependent on the voltage applied to ITO and the electrolyte composition, as reported in Fig. 15(b-c).

A 100 nm ITO film was also employed in (Okazaki et al., 2021, 2020) to coat an arc induced LPG (period 650 μm) and employed in a opto-electrochemical setup for the detection of mM concentrations of different electroactive species, i.e., methylene blue, hexaammineruthenium ($Ru(NH_3)_6^{3+}$), ferrocyanide, ferrocenedimethanol ($Fc(CH_2OH)_2$). Transmittance changes as a function of the applied potential and current values were measured, with the possibility to detect, for example, 0.001–1 mM concentrations of MB.

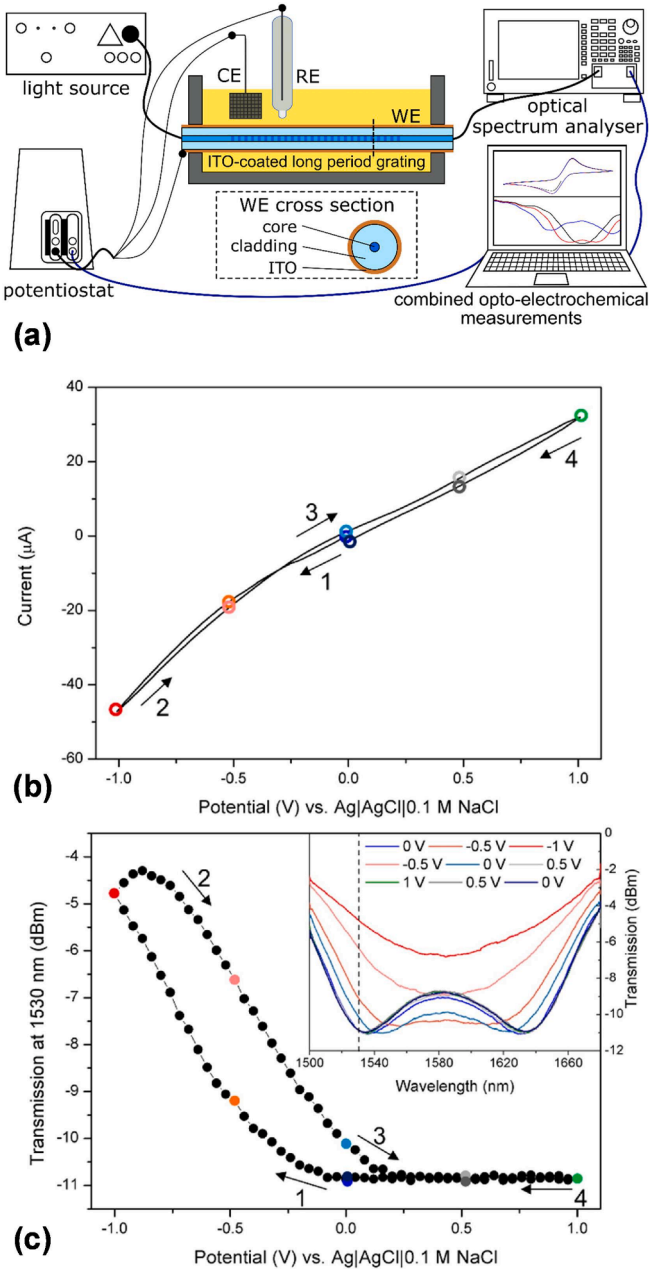

Fig. 15. LPG coated with ITO film: (a) Opto-electrochemical measurement setup; (b) CV response; (c) LPG optical transmission as a function of the potential. Adapted with permission from (Janczuk-Richter et al., 2019). © Elsevier.

4. Conclusions and outlooks

A detailed review regarding the state-of-the-art long period grating based chemical sensors was reported in this work. An extensive comparison of the literature has been provided, by grouping the works into macro-categories based on the target analytes. The emphasis was posed on the design, fabrication and characterization of the sensors and a detailed description was presented, by focusing the attention on transducer configurations, methodologies to increase the sensitivity and coating materials providing the selectivity to the considered targets.

To summarize, the most part of considered LPGs were written by using UV- or CO_2– laser techniques in standard single mode fibers. Anyway, unconventional designs and waveguides were also considered to increase the sensitivity and provide additional features, as for

example: PCF (J. Yang et al., 2017b), microfibers (T. Huang et al., 2021b) and etched fibers (Wu et al., 2016). Electric arc discharge fabrication method is also worth of mentioning in different cases (Coelho et al., 2015).

TAP LPGs are the most employed transducers due to their high SRI sensitivity (Hromadka et al., 2018a), while standard gratings coupling to high order cladding modes follow (Cusano et al., 2006b), often exploiting the mode transition phenomenon through the deposition of HRI overlays. Moreover, the use of cascaded LPGs forming interferometric configurations can be also found in some cases (Hao and Chiang, 2017).

Regarding sensitive nanomaterials, many configurations have been explored so far. Polyelectrolyte multilayers of PAH or PDDA with PAA or PSS, also with silica nanoparticles (SiO_2-NPs) (Korposh et al., 2012a; Viegas et al., 2009a; Wang et al., 2013) are probably the most widely considered. Several other polymer materials were considered, such as PVA (Alwis et al., 2013a), polyimide (Alwis et al., 2013b), polystyrene (Esposito et al., 2018d), PDMS (Barnes et al., 2010), polycarbonate (Yang et al., 2015) and hydrogels (Yang et al., 2019). Metal oxides like TiO_2 (Consales et al., 2014), SnO_2, Cu_2O (Monteiro-Silva et al., 2018), ZnO (Wu et al., 2016), WO_3 (Caucheteur et al., 2008) and ITO (Janczuk-Richter et al., 2019) are also worth to be highlighted, as well as metal organic frameworks (Hromadka et al., 2018a). Ag/Fe-C complexes have a prominent role regarding corrosion monitoring (Chen et al., 2016). Finally, novel 2D materials like graphene (Hao and Chiang, 2017) and graphene oxide (Xu et al., 2019) have been recently explored with interesting results.

The mentioned configurations permitted to detect a wide range of analytes, both in air and in solutions, as it can be inferred from Table 1. Many sensors focused on the detection of relative humidity (Viegas et al., 2011) and pH (Corres et al., 2007b). The detection of VOCs has been widely investigated by targeting, for example, acetone (Hromadka et al., 2018a), benzene (Topliss et al., 2010), chloroform (Cusano et al., 2006b), ethanol (Monteiro-Silva et al., 2018), methanol (Hromadka et al., 2015), toluene (Partridge et al., 2014), xylene (Yang et al., 2015), methane (Yang et al., 2015) and butane (Esposito et al., 2018d). Environmental and hazardous gases were also widely investigated, including: ammonia (Wang et al., 2016), carbon dioxide (Hromadka et al., 2018b), hydrogen (Caucheteur et al., 2008) and nitric oxide (Xu et al., 2019). Reports on the detection of heavy metal ions (e.g., arsenic, chromium, lead, mercury and nickel) can be also found in recent years (Wang et al., 2020a). Several other works focused on corrosion monitoring of steel bars (Chen et al., 2016) and measurement of marine salinity (F. Yang et al., 2017a). Applications to food quality assessment (Korposh et al., 2014) were also demonstrated. Nowadays, the development of multi-domain sensing equipment has been demonstrated, where the optical measurements are combined with electrical ones to provide additional information (Janczuk-Richter et al., 2019).

Based on these results achieved in the last 15/20 years it is possible to conclude that the LPG is a highly sensitive and flexible platform for the development of chemical sensors, with LODs down to few ppm.

Future research has to be focused on the following aspects. The multiplexing advantages of optical fiber technology need to be further exploited, through the design of different gratings in the same fiber for the measurement of multiple chemical species, similarly to what was reported in (Hromadka et al., 2017a). It should be highlighted here that, despite the enormous potential, LPGs have not shared the success of FBGs regarding the availability of commercial solutions. In this context, there are two main concerns which need to be addressed: the design of compact packaging solutions, able to keep the fiber in proper position and to eliminate/mitigate cross-sensitivities to environmental parameters (Esposito et al., 2018c; Qin et al., 2000); the development of low cost and compact interrogation systems (dos Santos et al., 2019). These approaches would provide a new impulse to the technology transfer from laboratory to market of LPG-based sensing technology.

Declaration of Competing Interest

The authors declare that they have no known competing financial interests or personal relationships that could have appeared to influence the work reported in this paper.

Acknowledgements

The author would like to thank Prof. Agostino Iadicicco and Prof. Stefania Campopiano for their suggestions and valuable support.

References

Allsop, T., Dubov, M., Martinez, A., Floreani, F., Khrushchev, I., Webb, D.J., Bennion, I., 2006. Bending characteristics of fiber long-period gratings with cladding index modified by femtosecond laser. J. Light. Technol. 24 (8), 3147–3154. https://doi.org/10.1109/JLT.2006.878037.

Allsop, T., Zhang, L., Bennion, I., 2001. Detection of organic aromatic compounds in paraffin by a long-period fiber grating optical sensor with optimized sensitivity. Opt. Commun. 191 (3-6), 181–190. https://doi.org/10.1016/S0030-4018(01)01131-2.

Alwis, L., Sun, T., Grattan, K.T.V., 2013a. Fibre optic long period grating-based humidity sensor probe using a Michelson interferometric arrangement. Sensors Actuators B Chem. 178, 694–699. https://doi.org/10.1016/j.snb.2012.11.062.

Alwis, L., Sun, T., Grattan, K.V., 2013b. Analysis of Polyimide-Coated Optical Fiber Long-Period Grating-Based Relative Humidity Sensor. IEEE Sens. J. 13 (2), 767–771. https://doi.org/10.1109/JSEN.2012.2227714.

Arjmand, M., Chiavaioli, F., Berneschi, S., Baldini, F., Soltanolkotabi, M., Trono, C., 2016. Effect of induced inner curvature on refractive index sensitivity in internally tilted long-period gratings. Opt. Lett. 41, 1443–1446. https://doi.org/10.1364/OL.41.001443.

Ascorbe, J., Corres, J., Arregui, F., Matias, I., 2017. Recent Developments in Fiber Optics Humidity Sensors. Sensors 17, 893. https://doi.org/10.3390/s17040893.

Barnes, J., Dreher, M., Plett, K., Brown, R.S., Crudden, C.M., Loock, H.-P., 2008. Chemical sensor based on a long-period fibre grating modified by a functionalized polydimethylsiloxane coating. Analyst 133, 1541–1549. https://doi.org/10.1039/b806129g.

Barnes, J.A., Brown, R.S., Cheung, A.H., Dreher, M.A., Mackey, G., Loock, H.-P., 2010. Chemical sensing using a polymer coated long-period fiber grating interrogated by ring-down spectroscopy. Sensors Actuators B Chem. 148 (1), 221–226. https://doi.org/10.1016/j.snb.2010.04.007.

Basumallick, N., Biswas, P., Carter, R.M., Maier, R.R.J., Bandyopadhyay, S., Dasgupta, K., Bandyopadhyay, S., 2016. Design of Palladium-Coated Long-Period Fiber Grating for Hydrogen Sensing. J. Light. Technol. 34 (21), 4912–4919. https://doi.org/10.1109/JLT.2016.2604481.

Berruti, G., Consales, M., Borriello, A., Giordano, M., Buontempo, S., Makovec, A., Breglio, G., Petagna, P., Cusano, A., 2014. A Comparative Study of Radiation-Tolerant Fiber Optic Sensors for Relative Humidity Monitoring in High-Radiation Environments at CERN. IEEE Photonics J. 6 (6), 1–15. https://doi.org/10.1109/JPHOT.2014.2357433.

Caucheteur, C., Debliquy, M., Lahem, D., Megret, P., 2008. Hybrid fiber gratings coated with a catalytic sensitive layer for hydrogen sensing in air. Opt. Express 16, 16854–16859. https://doi.org/10.1364/OE.16.016854.

Chen, X., Zhou, K., Zhang, L., Bennion, I., 2007. Dual-peak long-period fiber gratings with enhanced refractive index sensitivity by finely tailored mode dispersion that uses the light cladding etching technique. Appl. Opt. 46, 451–455. https://doi.org/10.1364/AO.46.000451.

Chen, Y., Tang, F., Bao, Y., Tang, Y., Chen, G., 2016. A Fe-C coated long-period fiber grating sensor for corrosion-induced mass loss measurement. Opt. Lett. 41, 2306–2309. https://doi.org/10.1364/OL.41.002306.

Chen, Y., Tang, F., Tang, Y., O'Keefe, M.J., Chen, G., 2017. Mechanism and sensitivity of Fe-C coated long period fiber grating sensors for steel corrosion monitoring of RC structures. Corros. Sci. 127, 70–81. https://doi.org/10.1016/j.corsci.2017.08.021.

Chiavaioli, F., Baldini, F., Tombelli, S., Trono, C., Giannetti, A., 2017a. Biosensing with optical fiber gratings. Nanophotonics 6, 663–679. https://doi.org/10.1515/nanoph-2016-0178.

Chiavaioli, F., Baldini, F., Trono, C., Period, L., Gratings, F., 2017b. Manufacturing and Spectral Features of Different Types of Long Period Fiber Gratings: Phase-Shifted, Turn-Around Point, Internally Tilted, and Pseudo-Random. Fibers 5, 29. https://doi.org/10.3390/fib5030029.

Chiavaioli, F., Biswas, P., Trono, C., Jana, S., Bandyopadhyay, S., Basumallick, N., Giannetti, A., Tombelli, S., Bera, S., Mallick, A., Baldini, F., 2015. Sol–Gel-Based Titania-Silica Thin Film Overlay for Long Period Fiber Grating-Based Biosensors. Anal. Chem. 87 (24), 12024–12031. https://doi.org/10.1021/acs.analchem.5b0184110.1021/acs.analchem.5b01841.s001.

Chiavaioli, F., Janner, D., 2021. Fiber Optic Sensing With Lossy Mode Resonances: Applications and Perspectives. J. Light. Technol. 39 (12), 3855–3870. https://doi.org/10.1109/JLT.2021.3052137.

Chiavaioli, F., Trono, C., Baldini, F., 2013. Specially designed long period grating with internal geometric bending for enhanced refractive index sensitivity. Appl. Phys. Lett. 102 (23), 231109. https://doi.org/10.1063/1.4810743.

Coelho, L.C.C., dos Santos, P.S.S., Jorge, P.A.d.S., Santos, J.L., de Almeida, J.M.M.M., 2018. Real-Time Early Warning Strategies for Corrosion Mitigation in Harsh

Environments. J. Light. Technol. 36 (4), 1152–1158. https://doi.org/10.1109/JLT.2017.2755076.
Coelho, L., Santos, J.L., Viegas, D., de Almeida, J.M.M.M., 2016. Fabrication and Characterization of Metal Oxide-Coated Long-Period Fiber Gratings. J. Light. Technol. 34 (10), 2533–2539. https://doi.org/10.1109/JLT.2016.2540358.
Coelho, L., Viegas, D., Santos, J.L., de Almeida, J.M.M.M., 2015. Detection of Extra Virgin Olive Oil Thermal Deterioration Using a Long Period Fibre Grating Sensor Coated with Titanium Dioxide. Food Bioprocess Technol. 8 (6), 1211–1217. https://doi.org/10.1007/s11947-015-1489-9.
Consales, M., Berruti, G., Borriello, A., Giordano, M., Buontempo, S., Breglio, G., Makovec, A., Petagna, P., Cusano, A., 2014. Nanoscale TiO2-coated LPGs as radiation-tolerant humidity sensors for high-energy physics applications. Opt. Lett. 39, 4128–4131. https://doi.org/10.1364/OL.39.004128.
Corres, J.M., del Villar, I., Matias, I.R., Arregui, F.J., 2007a. Fiber-optic pH-sensors in long-period fiber gratings using electrostatic self-assembly. Opt. Lett. 32, 29–31. https://doi.org/10.1364/OL.32.000029.
Corres, J.M., Matias, I.R., del Villar, I., Arregui, F.J., 2007b. Design of pH Sensors in Long-Period Fiber Gratings Using Polymeric Nanocoatings. IEEE Sens. J. 7 (3), 455–463. https://doi.org/10.1109/JSEN.2007.891933.
Cusano, A., Iadicicco, A., Pilla, P., Contessa, L., Campopiano, S., Cutolo, A., Giordano, M., 2006a. Mode transition in high refractive index coated long period gratings. Opt. Express 14, 19–34. https://doi.org/10.1364/OPEX.14.000019.
Cusano, A., Iadicicco, A., Pilla, P., Contessa, L., Campopiano, S., Cutolo, A., Giordano, M., Guerra, G., 2006b. Coated long-period fiber gratings as high-sensitivity optochemical sensors. J. Light. Technol. 24 (4), 1776–1786. https://doi.org/10.1109/JLT.2006.871128.
Dandapat, K., Kumar, I., Tripathi, S.M., 2021. Ultrahigh sensitive long-period fiber grating-based sensor for detection of adulterators in biofuel. Appl. Opt. 60, 7206–7213. https://doi.org/10.1364/AO.427495.
Del Villar, I., 2015. Ultrahigh-sensitivity sensors based on thin-film coated long period gratings with reduced diameter, in transition mode and near the dispersion turning point. Opt. Express 23, 8389–8398. https://doi.org/10.1364/OE.23.008389.
Del Villar, I., Cruz, J.L., Socorro, A.B., Corres, J.M., Matias, I.R., 2016. Sensitivity optimization with cladding-etched long period fiber gratings at the dispersion turning point. Opt. Express 24 (16), 17680. https://doi.org/10.1364/OE.24.01768010.1364/OE.24.017680.v00110.1364/OE.24.017680.v002.
Del Villar, I., Fuentes, O., Chiavaioli, F., Corres, J.M., Matias, I.R., 2018. Optimized Strain Long-Period Fiber Grating (LPFG) Sensors Operating at the Dispersion Turning Point. J. Light. Technol. 36 (11), 2240–2247. https://doi.org/10.1109/JLT.2018.2790434.
Del Villar, I., Matías, I., Arregui, F., Lalanne, P., 2005. Optimization of sensitivity in Long Period Fiber Gratings with overlay deposition. Opt. Express 13, 56–69. https://doi.org/10.1364/OPEX.13.000056.
Dey, T.K., Tombelli, S., Biswas, P., Giannetti, A., Basumallick, N., Baldini, F., Bandyopadhyay, S., Trono, C., 2021. Analysis of the Lowest Order Cladding Mode of Long Period Fiber Gratings Near Turn Around Point. J. Light. Technol. 39 (12), 4006–4012. https://doi.org/10.1109/JLT.2020.2987795.
Dissanayake, K.P.W., Wu, W., Nguyen, H., Sun, T., Grattan, K.T.V., 2018. Graphene-Oxide-Coated Long-Period Grating-Based Fiber Optic Sensor for Relative Humidity and External Refractive Index. J. Light. Technol. 36 (4), 1145–1151. https://doi.org/10.1109/JLT.2017.2756097.
dos Santos, P.S.S., Jorge, P.A.S., de Almeida, J., Coelho, L., 2019. Low-Cost Interrogation System for Long-Period Fiber Gratings Applied to Remote Sensing. Sensors 19, 1500. https://doi.org/10.3390/s19071500.
Du, J., Cipot-Wechsler, J., Lobez, J.M., Loock, H.-P., Crudden, C.M., 2010. Periodic Mesoporous Organosilica Films: Key Components of Fiber-Optic-Based Heavy-Metal Sensors. Small 6 (11), 1168–1172. https://doi.org/10.1002/smll.201000269.
Durr, F., Rego, G., Marques, P.V.S., Semjonov, S.L., Dianov, E.M., Limberger, H.G., Salathe, R.P., 2005. Tomographic stress profiling of arc-induced long-period fiber gratings. J. Light. Technol. 23 (11), 3947–3953. https://doi.org/10.1109/JLT.2005.857763.
Eftimov, T., Janik, M., Koba, M., Śmietana, M., Mikulic, P., Bock, W., 2020. Long-Period Gratings and Microcavity In-Line Mach Zehnder Interferometers as Highly Sensitive Optical Fiber Platforms for Bacteria Sensing. Sensors 20, 3772. https://doi.org/10.3390/s20133772.
Elosua, C., Arregui, F.J., Villar, I.D., Ruiz-Zamarreño, C., Corres, J.M., Bariain, C., Goicoechea, J., Hernaez, M., Rivero, P.J., Socorro, A.B., Urrutia, A., Sanchez, P., Zubiate, P., Lopez-Torres, D., Acha, N.D., Ascorbe, J., Ozcariz, A., Matias, I., 2017. Micro and Nanostructured Materials for the Development of Optical Fibre Sensors. Sensors 17, 2312. https://doi.org/10.3390/s17102312.
Esposito, F., Campopiano, S., Iadicicco, A., 2019a. Arc-Induced Long Period Gratings in Erbium-Doped Fiber. IEEE Photonics J. 11 (1), 1–8. https://doi.org/10.1109/JPHOT.2019.2894300.
Esposito, F., Ranjan, R., Campopiano, S., Iadicicco, A., 2018a. Arc-Induced Long Period Gratings from Standard to Polarization-Maintaining and Photonic Crystal Fibers. Sensors 18, 918. https://doi.org/10.3390/s18030918.
Esposito, F., Sansone, L., Srivastava, A., Baldini, F., Campopiano, S., Chiavaioli, F., Giordano, M., Giannetti, A., Iadicicco, A., 2021a. Long period grating in double cladding fiber coated with graphene oxide as high-performance optical platform for biosensing. Biosens. Bioelectron. 172, 112747. https://doi.org/10.1016/j.bios.2020.112747.
Esposito, F., Sansone, L., Srivastava, A., Cusano, A.M., Campopiano, S., Giordano, M., Iadicicco, A., 2021b. Label-free detection of vitamin D by optical biosensing based on long period fiber grating. Sensors Actuators B Chem. 347, 130637. https://doi.org/10.1016/j.snb.2021.130637.
Esposito, F., Sansone, L., Taddei, C., Campopiano, S., Giordano, M., Iadicicco, A., 2018b. Ultrasensitive biosensor based on long period grating coated with polycarbonate-graphene oxide multilayer. Sensors Actuators B Chem. 274, 517–526. https://doi.org/10.1016/j.snb.2018.08.002.
Esposito, F., Srivastava, A., Campopiano, S., Iadicicco, A., 2020a. Radiation Effects on Long Period Fiber Gratings: A Review. Sensors 20, 2729. https://doi.org/10.3390/s20092729.
Esposito, F., Srivastava, A., Iadicicco, A., Campopiano, S., 2019b. Multi-parameter sensor based on single Long Period Grating in Panda fiber for the simultaneous measurement of SRI, temperature and strain. Opt. Laser Technol. 113, 198–203. https://doi.org/10.1016/j.optlastec.2018.12.022.
Esposito, F., Srivastava, A., Sansone, L., Giordano, M., Campopiano, S., Iadicicco, A., 2021c. Label-Free Biosensors Based on Long Period Fiber Gratings: A Review. IEEE Sens. J. 21 (11), 12692–12705. https://doi.org/10.1109/JSEN.2020.3025488.
Esposito, F., Srivastava, A., Sansone, L., Giordano, M., Campopiano, S., Iadicicco, A., 2020b. Sensitivity Enhancement in Long Period Gratings by Mode Transition in Uncoated Double Cladding Fibers. IEEE Sens. J. 20 (1), 234–241. https://doi.org/10.1109/JSEN.736110.1109/JSEN.2019.2942639.
Esposito, F., Stancalie, A., Negut, C.-D., Campopiano, S., Sporea, D., Iadicicco, A., 2019c. Comparative Investigation of Gamma Radiation Effects on Long Period Gratings and Optical Power in Different Optical Fibers. J. Light. Technol. 37 (18), 4560–4566. https://doi.org/10.1109/JLT.5010.1109/JLT.2019.2910639.
Esposito, F., Zotti, A., Palumbo, G., Zuppolini, S., Consales, M., Cutolo, A., Borriello, A., Campopiano, S., Zarrelli, M., Iadicicco, A., 2018c. Liquefied Petroleum Gas Monitoring System Based on Polystyrene Coated Long Period Grating. Sensors 18, 1435. https://doi.org/10.3390/s18051435.
Esposito, F., Zotti, A., Ranjan, R., Zuppolini, S., Borriello, A., Campopiano, S., Zarrelli, M., Iadicicco, A., 2018d. Single-Ended Long Period Fiber Grating Coated With Polystyrene Thin Film for Butane Gas Sensing. J. Light. Technol. 36 (3), 825–832. https://doi.org/10.1109/JLT.2017.2776599.
Falate, R., Kamikawachi, R.C., Müller, M., Kalinowski, H.J., Fabris, J.L., 2005. Fiber optic sensors for hydrocarbon detection. Sensors Actuators B Chem. 105 (2), 430–436. https://doi.org/10.1016/j.snb.2004.06.033.
Guo, C., Fan, L., Chen, G., 2020. Corrosion-Induced Mass Loss Measurement under Strain Conditions through Gr/AgNW-Based. Fe-C Coated LPFG Sensors. Sensors 20, 1598. https://doi.org/10.3390/s20061598.
Guo, T., Liu, F., Guan, B.-O., Albert, J., 2016. Tilted fiber grating mechanical and biochemical sensors. Opt. Laser Technol. 78, 19–33. https://doi.org/10.1016/j.optlastec.2015.10.007.
Hao, T., Chiang, K.S., 2017. Graphene-Based Ammonia-Gas Sensor Using In-Fiber Mach-Zehnder Interferometer. IEEE Photonics Technol. Lett. 29 (23), 2035–2038. https://doi.org/10.1109/LPT.2017.2761981.
Heck, M., Schwartz, G., Krämer, R.G., Richter, D., Goebel, T.A., Matzdorf, C., Tünnermann, A., Nolte, S., 2019. Control of higher-order cladding mode excitation with tailored femtosecond-written long period fiber gratings. Opt. Express 27, 4292–4303. https://doi.org/10.1364/OE.27.004292.
Hernaez, M., Zamarreño, C., Melendi-Espina, S., Bird, L., Mayes, A., Arregui, F., 2017. Optical Fibre Sensors Using Graphene-Based Materials: A Review. Sensors 17, 155. https://doi.org/10.3390/s17010155.
Hromadka, J., Korposh, S., Partridge, M., James, S., Davis, F., Crump, D., Tatam, R., 2017a. Volatile Organic Compounds Sensing Using Optical Fibre Long Period Grating with Mesoporous Nano-Scale Coating. Sensors 17, 205. https://doi.org/10.3390/s17020205.
Hromadka, J., Korposh, S., Partridge, M.C., James, S.W., Davis, F., Crump, D., Tatam, R. P., 2017b. Multi-parameter measurements using optical fibre long period gratings for indoor air quality monitoring. Sensors Actuators B Chem. 244, 217–225. https://doi.org/10.1016/j.snb.2016.12.050.
Hromadka, J., Tokay, B., Correia, R., Morgan, S.P., Korposh, S., 2018a. Highly sensitive volatile organic compounds vapour measurements using a long period grating optical fibre sensor coated with metal organic framework ZIF-8. Sensors Actuators B Chem. 260, 685–692. https://doi.org/10.1016/j.snb.2018.01.015.
Hromadka, J., Tokay, B., Correia, R., Morgan, S.P., Korposh, S., 2018b. Carbon dioxide measurements using long period grating optical fibre sensor coated with metal organic framework HKUST-1. Sensors Actuators B Chem. 255, 2483–2494. https://doi.org/10.1016/j.snb.2017.09.041.
Hromadka, J., Tokay, B., James, S., Tatam, R.P., Korposh, S., 2015. Optical fibre long period grating gas sensor modified with metal organic framework thin films. Sensors Actuators B Chem. 221, 891–899. https://doi.org/10.1016/j.snb.2015.07.027.
Huang, C., Zhou, Y., Yu, G., Zeng, J., Li, Q., Shen, K., Wu, X., Guo, R., Zhang, C., Zheng, B., Wang, J., 2021a. Glutathione-functionalized long-period fiber gratings sensor based on surface plasmon resonance for detection of As3+ ions. Nanotechnology. https://doi.org/10.1088/1361-6528/ac1b56.
Huang, T., Fu, Q., Sun, L.-P., Liu, P., Wu, Z.e., Li, K., Xiao, R., Yang, X., Huang, Y., Lin, W., Lu, H., Ma, J., Wang, W., Li, J., Tang, Y., Guan, B.-O., 2021b. Photothermal lateral flow immunoassay using microfiber long-period grating. Sensors Actuators B Chem. 344, 130283. https://doi.org/10.1016/j.snb.2021.130283.
Huang, Y., Gao, Z., Chen, G., Xiao, H., 2013. Long period fiber grating sensors coated with nano iron/silica particles for corrosion monitoring. Smart Mater. Struct. 22 (7), 075018. https://doi.org/10.1088/0964-1726/22/7/075018.
Huang, Y., Tang, F., Liang, X., Chen, G., Xiao, H., Azarmi, F., 2015. Steel bar corrosion monitoring with long-period fiber grating sensors coated with nano iron/silica particles and polyurethane. Struct. Heal. Monit. 14 (2), 178–189. https://doi.org/10.1177/1475921714560070.
Iadicicco, A., Cusano, A., Campopiano, S., Cutolo, A., Giordano, M., 2005. Thinned fiber Bragg gratings as refractive index sensors. IEEE Sens. J. 5 (6), 1288–1295. https://doi.org/10.1109/JSEN.2005.859288.

Iadicicco, A., Ranjan, R., Campopiano, S., 2015. Fabrication and Characterization of Long Period Gratings in Hollow Core Fibers by Electric Arc Discharge. IEEE Sens. J. 15 (5), 3014–3020. https://doi.org/10.1109/JSEN.2014.2383175.
James, S.W., Tatam, R.P., 2003. Optical fibre long-period grating sensors: characteristics and application. Meas. Sci. Technol. 14 (5), R49–R61. https://doi.org/10.1088/0957-0233/14/5/201.
Janczuk-Richter, M., Piestrzyńska, M., Burnat, D., Sezemsky, P., Stranak, V., Bock, W.J., Bogdanowicz, R., Niedziółka-Jönsson, J., Śmietana, M., 2019. Optical investigations of electrochemical processes using a long-period fiber grating functionalized by indium tin oxide. Sensors Actuators B Chem. 279, 223–229. https://doi.org/10.1016/j.snb.2018.10.001.
Jiang, C., Liu, Y., Zhao, Y., Mou, C., Wang, T., 2019. Helical Long-Period Gratings Inscribed in Polarization-Maintaining Fibers by CO2 Laser. J. Light. Technol. 37 (3), 889–896. https://doi.org/10.1109/JLT.2018.2883376.
Jiang, H., Yang, R., Tang, X., Burnett, A., Lan, X., Xiao, H., Dong, J., 2013. Multilayer fiber optic sensors for in situ gas monitoring in harsh environments. Sensors Actuators B Chem. 177, 205–212. https://doi.org/10.1016/j.snb.2012.10.122.
Khan, S., Le Calvé, S., Newport, D., 2020. A review of optical interferometry techniques for VOC detection. Sensors Actuators A Phys. 302, 111782. https://doi.org/10.1016/j.sna.2019.111782.
Konstantaki, M., Klini, A., Anglos, D., Pissadakis, S., 2012. An ethanol vapor detection probe based on a ZnO nanorod coated optical fiber long period grating. Opt. Express 20, 8472–8484. https://doi.org/10.1364/OE.20.008472.
Konstantaki, M., Skiani, D., Vurro, D., Cucinotta, A., Selleri, S., Secchi, A., Iannotta, S., Pissadakis, S., 2020. Silk Fibroin Enabled Optical Fiber Methanol Vapor Sensor. IEEE Photonics Technol. Lett. 32 (9), 514–517. https://doi.org/10.1109/LPT.6810.1109/LPT.2020.2982451.
Korposh, S., Lee, S.-W., James, S., 2017. Long Period Grating Based Fibre Optic Chemical Sensors. In: Matias, I.R., Ikezawa, S., Corres, J. (Eds.), Fiber Optic Sensors: Current Status and Future Possibilities. Springer International Publishing, Cham, pp. 241–267. https://doi.org/10.1007/978-3-319-42625-9_12.
Korposh, S., Selyanchyn, R., James, S., Tatam, R., Lee, S.-W., 2014. Identification and quality assessment of beverages using a long period grating fibre-optic sensor modified with a mesoporous thin film. Sens. Bio-Sensing Res. 1, 26–33. https://doi.org/10.1016/j.sbsr.2014.06.001.
Korposh, S., Selyanchyn, R., Yasukochi, W., Lee, S.-W., James, S.W., Tatam, R.P., 2012a. Optical fibre long period grating with a nanoporous coating formed from silica nanoparticles for ammonia sensing in water. Mater. Chem. Phys. 133 (2-3), 784–792. https://doi.org/10.1016/j.matchemphys.2012.01.094.
Korposh, S., Wang, T., James, S., Tatam, R., Lee, S.-W., 2012b. Pronounced aromatic carboxylic acid detection using a layer-by-layer mesoporous coating on optical fibre long period grating. Sensors Actuators B Chem. 173, 300–309. https://doi.org/10.1016/j.snb.2012.07.005.
Kreno, L.E., Leong, K., Farha, O.K., Allendorf, M., Van Duyne, R.P., Hupp, J.T., 2012. Metal-Organic Framework Materials as Chemical Sensors. Chem. Rev. 112 (2), 1105–1125. https://doi.org/10.1021/cr200324t.
Li, W., Miao, Y., Fei, C., Zhang, H., Li, B., Zhang, K., 2021. Enhanced photothermal signal detection by graphene oxide integrated long period fiber grating for on-site quantification of sodium copper chlorophyllin. Analyst 146 (11), 3617–3622. https://doi.org/10.1039/D1AN00444A.
Liu, Y., Peng, W., 2021. Fiber-Optic Surface Plasmon Resonance Sensors and Biochemical Applications: A Review. J. Light. Technol. 39 (12), 3781–3791. https://doi.org/10.1109/JLT.2020.3045068.
Liu, Z., Liu, Y., Mou, C., Zou, F., Wang, T., 2018. CO2 laser-written long-period fiber grating with a high diffractive order cladding mode near the turning point. Appl. Opt. 57, 4756–4760. https://doi.org/10.1364/AO.57.004756.
Lobry, M., Fasseaux, H., Loyez, M., Chah, K., Goormaghtigh, E., Wattiez, R., Chiavaioli, F., Caucheteur, C., 2021. Plasmonic fiber grating biosensors demodulated through spectral envelopes intersection. J. Light. Technol. 39 (22), 7288–7295. https://doi.org/10.1109/JLT.2021.311285410.1109/JLT.2021.3112854/mm1.
McDonagh, C., Burke, C.S., MacCraith, B.D., 2008. Optical Chemical Sensors. Chem. Rev. 108 (2), 400–422. https://doi.org/10.1021/cr068102g.
Melo, L., Burton, G., Davies, B., Risk, D., Wild, P., 2014. Highly sensitive coated long period grating sensor for CO2 detection at atmospheric pressure. Sensors Actuators B Chem. 202, 294–300. https://doi.org/10.1016/j.snb.2014.05.062.
Mensitieri, G., Venditto, V., Guerra, G., 2003. Polymeric sensing films absorbing organic guests into a nanoporous host crystalline phase. Sensors Actuators B Chem. 92 (3), 255–261. https://doi.org/10.1016/S0925-4005(03)00273-9.
Miliou, A., 2021. In-Fiber Interferometric-Based Sensors: Overview and Recent Advances. Photonics 8, 265. https://doi.org/10.3390/photonics8070265.
Mishra, S.K., Chiang, K.S., 2020. Phenolic-compounds sensor based on immobilization of tyrosinase in polyacrylamide gel on long-period fiber grating. Opt. Laser Technol. 131, 106464. https://doi.org/10.1016/j.optlastec.2020.106464.
Mishra, S.K., Zou, B., Chiang, K.S., 2017. Wide-Range pH Sensor Based on a Smart-Hydrogel-Coated Long-Period Fiber Grating. IEEE J. Sel. Top. Quantum Electron. 23 (2), 284–288. https://doi.org/10.1109/JSTQE.2016.2629662.
Monteiro-Silva, F., Santos, J.L., de Almeida, J.M.M.M., Coelho, L., 2018. Quantification of Ethanol Concentration in Gasoline Using Cuprous Oxide Coated Long Period Fiber Gratings. IEEE Sens. J. 18 (4), 1493–1500. https://doi.org/10.1109/JSEN.736110.1109/JSEN.2017.2782566.
Okazaki, T., Orii, T., Tan, S.-Y., Watanabe, T., Taguchi, A., Rahman, F.A., Kuramitz, H., 2020. Electrochemical Long Period Fiber Grating Sensing for Electroactive Species. Anal. Chem. 92 (14), 9714–9721. https://doi.org/10.1021/acs.analchem.0c0106210.1021/acs.analchem.0c01062.s001.
Okazaki, T., Orii, T., Tan, S., Watanabe, T., Taguchi, A., Rahman, F.A., Kuramitz, H., 2021. Potential-Scanning Sensing for Refractive Index Using an Indium Tin Oxide (ITO)-Coated Long-Period Fiber Grating (LPFG). Anal. Lett. https://doi.org/10.1080/00032719.2021.1951749.
Partridge, M., James, S.W., Tatam, R.P., 2016. Dissolved Oxygen Sensing Using an Optical Fiber Long Period Grating Coated With Hemoglobin. J. Light. Technol. 34 (19), 4506–4510. https://doi.org/10.1109/JLT.5010.1109/JLT.2016.2533161.
Partridge, M., Wong, R., James, S.W., Davis, F., Higson, S.P.J., Tatam, R.P., 2014. Long period grating based toluene sensor for use with water contamination. Sensors Actuators B Chem. 203, 621–625. https://doi.org/10.1016/j.snb.2014.06.121.
Pawar, D., Kale, S.N., 2019. A review on nanomaterial-modified optical fiber sensors for gases, vapors and ions. Microchim. Acta 186, 253. https://doi.org/10.1007/s00604-019-3351-7.
Peshko, I., Cherry, O., Rutkevich, T., Hockley, B., Rubtsov, V., 2005. Long-period gratings in optical fibres for chemical sensor applications. Meas. Sci. Technol. 16 (11), 2221–2228. https://doi.org/10.1088/0957-0233/16/11/013.
Piestrzyńska, M., Dominik, M., Kosiel, K., Janczuk-Richter, M., Szot-Karpińska, K., Brzozowska, E., Shao, L., Niedziółka-Jonsson, J., Bock, W.J., Śmietana, M., 2019. Ultrasensitive tantalum oxide nano-coated long-period gratings for detection of various biological targets. Biosens. Bioelectron. 133, 8–15. https://doi.org/10.1016/j.bios.2019.03.006.
Pilla, P., Foglia Manzillo, P., Giordano, M., Korwin-Pawlowski, M.L., Bock, W.J., Cusano, A., 2008. Spectral behavior of thin film coated cascaded tapered long period gratings in multiple configurations. Opt. Express 16, 9765–9780. https://doi.org/10.1364/OE.16.009765.
Pilla, P., Iadicicco, A., Contessa, L., Campopiano, S., Cutolo, A., Giordano, M., Guerra, G., Cusano, A., 2005. Optical chemo-sensor based on long period gratings coated with delta form syndiotactic polystyrene. IEEE Photonics Technol. Lett. 17, 1713–1715. https://doi.org/10.1109/LPT.2005.851979.
Pilla, P., Trono, C., Baldini, F., Chiavaioli, F., Giordano, M., Cusano, A., 2012. Giant sensitivity of long period gratings in transition mode near the dispersion turning point: an integrated design approach. Opt. Lett. 37, 4152–4154. https://doi.org/10.1364/OL.37.004152.
Possetti, G.R.C., Kamikawachi, R.C., Prevedello, C.L., Muller, M., Fabris, J.L., 2009. Salinity measurement in water environment with a long period grating based interferometer. Meas. Sci. Technol. 20 (3), 034003. https://doi.org/10.1088/0957-0233/20/3/034003.
Qin, L., Wei, Z.X., Wang, Q.Y., Li, H.P., Zheng, W., Zhang, Y.S., Gao, D.S., 2000. Compact temperature-compensating package for long-period fiber gratings. Opt. Mater. (Amst) 14 (3), 239–242. https://doi.org/10.1016/S0925-3467(99)00144-5.
Qin, X., Feng, W., Yang, X., Wei, J., Huang, G., 2018. Molybdenum sulfide/citric acid composite membrane-coated long period fiber grating sensor for measuring trace hydrogen sulfide gas. Sensors Actuators B Chem. 272, 60–68. https://doi.org/10.1016/j.snb.2018.05.152.
Quero, G., Consales, M., Severino, R., Vaiano, P., Boniello, A., Sandomenico, A., Ruvo, M., Borriello, A., Diodato, L., Zuppolini, S., Giordano, M., Nettore, I.C., Mazzarella, C., Colao, A., Macchia, P.E., Santorelli, F., Cutolo, A., Cusano, A., 2016. Long period fiber grating nano-optrode for cancer biomarker detection. Biosens. Bioelectron. 80, 590–600. https://doi.org/10.1016/j.bios.2016.02.021.
Quero, G., Crescitelli, A., Paladino, D., Consales, M., Buosciolo, A., Giordano, M., Cutolo, A., Cusano, A., 2011. Evanescent wave long-period fiber grating within D-shaped optical fibers for high sensitivity refractive index detection. Sensors Actuators B Chem. 152 (2), 196–205. https://doi.org/10.1016/j.snb.2010.12.007.
Ranjan, R., Esposito, F., Iadicicco, A., Campopiano, S., 2017. Arc-Induced Long Period Gratings in Phosphorus-Doped Fiber. IEEE Photonics Technol. Lett. 29 (7), 611–614. https://doi.org/10.1109/LPT.6810.1109/LPT.2017.2675161.
Rego, G., 2016. Arc-Induced Long Period Fiber Gratings. J. Sensors 2016, 1–14. https://doi.org/10.1155/2016/3598634.
Rego, G., Caldas, P., Ivanov, O.V., 2021. Arc-Induced Long-Period Fiber Gratings at INESC TEC. Part I: Fabrication. Characterization and Mechanisms of Formation. Sensors 21, 4914. https://doi.org/10.3390/s21144914.
Rego, G., Falate, R., Santos, J.L., Salgado, H.M., Fabris, J.L., Semjonov, S.L., Dianov, E. M., 2005a. Arc-induced long-period gratings in aluminosilicate glass fibers. Opt. Lett. 30, 2065–2067. https://doi.org/10.1364/OL.30.002065.
Rego, G., Fernandez Fernandez, A., Gusarov, A., Brichard, B., Berghmans, F., Santos, J.L., Salgado, H.M., 2005b. Effect of ionizing radiation on the properties of arc-induced long-period fiber gratings. Appl. Opt. 44, 6258–6263. https://doi.org/10.1364/AO.44.006258.
Ren, K., Ren, L., Liang, J., Kong, X., Ju, H., Wu, Z., 2017. Highly Strain and Bending Sensitive Microtapered Long-Period Fiber Gratings. IEEE Photonics Technol. Lett. 29 (13), 1085–1088. https://doi.org/10.1109/LPT.2017.2702573.
Rivero, P., Goicoechea, J., Arregui, F., 2019. Layer-by-Layer Nano-assembly: A Powerful Tool for Optical Fiber Sensing Applications. Sensors 19, 683. https://doi.org/10.3390/s19030683.
Rodríguez-Garciapiña, J.L., Beltrán-Pérez, G., Castillo-Mixcóatl, J., Muñoz-Aguirre, S., 2021. Application of the principal components analysis technique to optical fiber sensors for acetone detection. Opt. Laser Technol. 143, 107314. https://doi.org/10.1016/j.optlastec.2021.107314.
Sharma, A.K., Pandey, A.K., Kaur, B., 2018. A Review of advancements (2007–2017) in plasmonics-based optical fiber sensors. Opt. Fiber Technol. 43, 20–34. https://doi.org/10.1016/j.yofte.2018.03.008.
Shu, X., Allsop, T., Gwandu, B., Zhang, L., Bennion, I., 2001. High-temperature sensitivity of long-period gratings in B-Ge codoped fiber. IEEE Photonics Technol. Lett. 13, 818–820. https://doi.org/10.1109/68.935814.
Shu, X., Zhang, L., Bennion, I., 2002. Sensitivity characteristics of long-period fiber gratings. J. Light. Technol. 20, 255–266. https://doi.org/10.1109/50.983240.
Śmietana, M., Koba, M., Mikulic, P., Bock, W.J., 2016. Towards refractive index sensitivity of long-period gratings at level of tens of μm per refractive index unit:

fiber cladding etching and nano-coating deposition. Opt. Express 24, 11897–11904. https://doi.org/10.1364/OE.24.011897.
Srivastava, A., Esposito, F., Campopiano, S., Iadicicco, A., 2019. Fabrication and characterization of long period gratings in pure-silica fibers, in: Lieberman, R.A., Baldini, F., Homola, J. (Eds.), Proc. SPIE 11028, Optical Sensors 2019. SPIE, p. 110282E. https://doi.org/10.1117/12.2521604.
Srivastava, A., Esposito, F., Pereira, J.M.B., Campopiano, S., Iadicicco, A., 2020. Fabrication and characterization of arc-induced long period gratings in optical fibers with micro-channels, in: 2020 IEEE Sensors. IEEE, pp. 1–4. https://doi.org/10.1109/SENSORS47125.2020.9278736.
Stăncălie, A., Sporea, D., Neguţ, D., Esposito, F., Ranjan, R., Campopiano, S., Iadicicco, A., 2018. Long Period Gratings in unconventional fibers for possible use as radiation dosimeter in high-dose applications. Sensors Actuators A Phys. 271, 223–229. https://doi.org/10.1016/j.sna.2018.01.034.
Subramanian, R., Zhu, C., Zhao, H., Li, H., 2018. Torsion, Strain, and Temperature Sensor Based on Helical Long-Period Fiber Gratings. IEEE Photonics Technol. Lett. 30 (4), 327–330. https://doi.org/10.1109/LPT.2017.2787157.
Tan, S.-Y., Lee, S.-C., Okazaki, T., Kuramitz, H., Abd-Rahman, F., 2018. Detection of mercury (II) ions in water by polyelectrolyte–gold nanoparticles coated long period fiber grating sensor. Opt. Commun. 419, 18–24. https://doi.org/10.1016/j.optcom.2018.02.069.
Tang, F., Chen, Y., Li, Z., Tang, Y., Chen, G., 2018. Application of Fe-C coated LPFG sensor for early stage corrosion monitoring of steel bar in RC structures. Constr. Build. Mater. 175, 14–25. https://doi.org/10.1016/j.conbuildmat.2018.04.187.
Tang, X., Provenzano, J., Xu, Z., Dong, J., Duan, H., Xiao, H., 2011. Acidic ZSM-5 zeolite-coated long period fiber grating for optical sensing of ammonia. J. Mater. Chem. 21 (1), 181–186. https://doi.org/10.1039/C0JM02523B.
Tang, X., Remmel, K., Lan, X., Deng, J., Xiao, H., Dong, J., 2009. Perovskite-Type Oxide Thin Film Integrated Fiber Optic Sensor for High-Temperature Hydrogen Measurement. Anal. Chem. 81 (18), 7844–7848. https://doi.org/10.1021/ac9012754.
Theodosiou, A., Min, R., Leal-Junior, A.G., Ioannou, A., Frizera, A., Pontes, M.J., Marques, C., Kalli, K., 2019. Long period grating in a multimode cyclic transparent optical polymer fiber inscribed using a femtosecond laser. Opt. Lett. 44, 5346–5349. https://doi.org/10.1364/OL.44.005346.
Thomas Lee, S., Dinesh Kumar, R., Suresh Kumar, P., Radhakrishnan, P., Vallabhan, C.P. G., Nampoori, V.P.N., 2003. Long period gratings in multimode optical fibers: application in chemical sensing. Opt. Commun. 224 (4-6), 237–241. https://doi.org/10.1016/S0030-4018(03)01597-9.
Topliss, S.M., James, S.W., Davis, F., Higson, S.P.J., Tatam, R.P., 2010. Optical fibre long period grating based selective vapour sensing of volatile organic compounds. Sensors Actuators B Chem. 143 (2), 629–634. https://doi.org/10.1016/j.snb.2009.10.008.
Tsai, Y.-T., Wu, C.-W., Tsai, L., Chiang, C.-C., 2021. Application of Graphene Oxide-Based, Long-Period Fiber Grating for Sensing Relative Humidity. J. Light. Technol. 39 (12), 4124–4130. https://doi.org/10.1109/JLT.2020.3006380.
Urrutia, A., Del Villar, I., Zubiate, P., Zamarreño, C.R., 2019. A Comprehensive Review of Optical Fiber Refractometers: Toward a Standard Comparative Criterion. Laser Photon. Rev. 13 (11), 1900094. https://doi.org/10.1002/lpor.v13.1110.1002/lpor.201900094.
Vaiano, P., Carotenuto, B., Pisco, M., Ricciardi, A., Quero, G., Consales, M., Crescitelli, A., Esposito, E., Cusano, A., 2016. Lab on Fiber Technology for biological sensing applications. Laser Photon. Rev. 10 (6), 922–961. https://doi.org/10.1002/lpor.201600111.
Venugopalan, T., Yeo, T.L., Sun, T., Grattan, K.T.V., 2008. LPG-Based PVA Coated Sensor for Relative Humidity Measurement. IEEE Sens. J. 8 (7), 1093–1098. https://doi.org/10.1109/JSEN.2008.926524.
Viegas, D., Goicoechea, J., Corres, J.M., Santos, J.L., Ferreira, L.A., Araújo, F.M., Matias, I.R., 2009a. A fibre optic humidity sensor based on a long-period fibre grating coated with a thin film of SiO2 nanospheres. Meas. Sci. Technol. 20 (3), 034002. https://doi.org/10.1088/0957-0233/20/3/034002.
Viegas, D., Goicoechea, J., Santos, J.L., Araújo, F.M., Ferreira, L.A., Arregui, F., Matias, I., 2009b. Sensitivity Improvement of a Humidity Sensor Based on Silica Nanospheres on a Long-Period Fiber Grating. Sensors 9, 519–527. https://doi.org/10.3390/s90100519.
Viegas, D., Hernaez, M., Goicoechea, J., Santos, J.L., Araujo, F.M., Arregui, F., Matias, I. R., 2011. Simultaneous Measurement of Humidity and Temperature Based on an SiO2-Nanospheres Film Deposited on a Long-Period Grating In-Line With a Fiber Bragg Grating. IEEE Sens. J. 11, 162–166. https://doi.org/10.1109/JSEN.2010.2055237.
Vitoria, I., Ruiz Zamarreño, C., Ozcariz, A., Matias, I.R., 2021. Fiber Optic Gas Sensors Based on Lossy Mode Resonances and Sensing Materials Used Therefor: A Comprehensive Review. Sensors 21, 731. https://doi.org/10.3390/s21030731.
Viveiros, D., de Almeida, J.M.M.M., Coelho, L., Vasconcelos, H., Maia, J.M., Amorim, V. A., Jorge, P.A.S., Marques, P.V.S., 2021. Turn Around Point Long Period Fiber Gratings With Coupling to Asymmetric Cladding Modes Fabricated by a Femtosecond Laser and Coated With Titanium Dioxide. J. Light. Technol. 39 (14), 4784–4793. https://doi.org/10.1109/JLT.2021.3078257.
Wang, R., Ren, Z., Kong, D., Wu, H., Hu, B., He, Z., 2020a. Graphene oxide functionalized micro-tapered long-period fiber grating for sensitive heavy metal sensing. Appl. Phys. Express 13, 067001. https://doi.org/10.35848/1882-0786/ab8b53.
Wang, R., Ren, Z., Kong, X., Kong, D., Hu, B., He, Z., 2020b. Graphene-assisted high-precision temperature sensing by long-period fiber gratings. J. Phys. D. Appl. Phys. 53 (6), 065104. https://doi.org/10.1088/1361-6463/ab5498.
Wang, T., Korposh, S., James, S., Tatam, R., Lee, S., 2013. Optical fiber long period grating sensor with a polyelectrolyte alternate thin film for gas sensing of amine odors. Sensors Actuators B Chem. 185, 117–124. https://doi.org/10.1016/j.snb.2013.04.034.
Wang, T., Yasukochi, W., Korposh, S., James, S.W., Tatam, R.P., Lee, S.-W., 2016. A long period grating optical fiber sensor with nano-assembled porphyrin layers for detecting ammonia gas. Sensors Actuators B Chem. 228, 573–580. https://doi.org/10.1016/j.snb.2016.01.058.
Wang, X.-D., Wolfbeis, O.S., 2020. Fiber-Optic Chemical Sensors and Biosensors (2015–2019). Anal. Chem. 92 (1), 397–430. https://doi.org/10.1021/acs.analchem.9b04708.
Wei, W., Nong, J., Zhang, G., Tang, L., Jiang, X., Chen, N., Luo, S., Lan, G., Zhu, Y., 2016. Graphene-Based Long-Period Fiber Grating Surface Plasmon Resonance Sensor for High-Sensitivity Gas Sensing. Sensors 17, 2. https://doi.org/10.3390/s17010002.
Wen, H.-Y., Wang, S.-H., Tsai, L., Hsu, R.-Y., Chiang, C.-C., 2020. Advanced NO Sensors on Notched Long-Period Fiber Gratings Covered by Mesoporous WO3. IEEE Sens. J. 20 (9), 4595–4601. https://doi.org/10.1109/JSEN.736110.1109/JSEN.2020.2965542.
Wu, C.-W., Wu, C.-C., Chiang, C.-C., 2016. A ZnO Nanoparticle-Coated Long Period Fiber Grating as a Carbon Dioxide Gas Sensor. Inventions 1, 21. https://doi.org/10.3390/inventions1040021.
Wu, J.-W., Chiang, C.-C., 2015. Notched Long-Period Fiber Grating with an Amine-Modified Surface Nanostructure for Carbon Dioxide Gas Sensing. Materials (Basel). 8, 4535–4543. https://doi.org/10.3390/ma8074535.
Wu, J., Tang, C., Zhang, W., Ma, X., Qu, S., Chen, K., Hao, T., Chiang, K.S., 2021. Lab on optical fiber: surface nano-functionalization for real-time monitoring of VOC adsorption/desorption in metal-organic frameworks. Nanophotonics 10 (10), 2705–2716. https://doi.org/10.1515/nanoph-2021-0192.
Xu, B., Huang, J., Ding, L., Zhang, H., Zhang, H., 2021. A sensitive ammonia sensor using long period fiber grating coated with graphene oxide/cellulose acetate. IEEE Sens. J. 21 (15), 16691–16700. https://doi.org/10.1109/JSEN.2021.3081745.
Xu, B., Huang, J., Xu, X., Zhou, A.i., Ding, L., 2019. Ultrasensitive NO Gas Sensor Based on the Graphene Oxide-Coated Long-Period Fiber Grating. ACS Appl. Mater. Interfaces 11 (43), 40868–40874. https://doi.org/10.1021/acsami.9b1421210.1021/acsami.9b14212.s001.
Yang, F., Hlushko, R., Wu, D.i., Sukhishvili, S.A., Du, H., Tian, F., 2019. Ocean Salinity Sensing Using Long-Period Fiber Gratings Functionalized with Layer-by-Layer Hydrogels. ACS Omega 4 (1), 2134–2141. https://doi.org/10.1021/acsomega.8b02823.
Yang, F., Sukhishvili, S., Du, H., Tian, F., 2017a. Marine salinity sensing using long-period fiber gratings enabled by stimuli-responsive polyelectrolyte multilayers. Sensors Actuators B Chem. 253, 745–751. https://doi.org/10.1016/j.snb.2017.06.121.
Yang, J., Che, X., Shen, R., Wang, C., Li, X., Chen, W., 2017b. High-sensitivity photonic crystal fiber long-period grating methane sensor with cryptophane-A-6Me absorbed on a PAA-CNTs/PAH nanofilm. Opt. Express 25, 20258–20267. https://doi.org/10.1364/OE.25.020258.
Yang, J., Tao, C., Li, X., Zhu, G., Chen, W., 2011. Long-period fiber grating sensor with a styrene-acrylonitrile nano-film incorporating cryptophane A for methane detection. Opt. Express 19, 14696–14706. https://doi.org/10.1364/OE.19.014696.
Yang, J., Zhou, L., Huang, J., Tao, C., Li, X., Chen, W., 2015. Sensitivity enhancing of transition mode long-period fiber grating as methane sensor using high refractive index polycarbonate/cryptophane A overlay deposition. Sensors Actuators B Chem. 207, 477–480. https://doi.org/10.1016/j.snb.2014.10.013.
Yang, Y., 2014. pH-sensing properties of cascaded long- and short-period fiber grating with poly acrylic acid/poly allylamine hydrochloride thin-film overlays. Opt. Eng. 53 (11), 116112. https://doi.org/10.1117/1.OE.53.11.116112.
Yin, M., Gu, B., An, Q.-F., Yang, C., Guan, Y.L., Yong, K.-T., 2018. Recent development of fiber-optic chemical sensors and biosensors: Mechanisms, materials, micro/nano-fabrications and applications. Coord. Chem. Rev. 376, 348–392. https://doi.org/10.1016/j.ccr.2018.08.001.
Zhang, J., Tang, X., Dong, J., Wei, T., Xiao, H., 2009. Zeolite thin film-coated long period fiber grating sensor for measuring trace organic vapors. Sensors Actuators B Chem. 135 (2), 420–425. https://doi.org/10.1016/j.snb.2008.09.033.
Zhang, X., Liu, Y., Wang, Z., Yu, J., Zhang, H., 2018. LP01-LP11a mode converters based on long-period fiber gratings in a two-mode polarization-maintaining photonic crystal fiber. Opt. Express 26, 7013–7021. https://doi.org/10.1364/OE.26.007013.
Zhao, X.-W., Wang, Q.i., 2019. Mini review: Recent advances in long period fiber grating biological and chemical sensors. Instrum. Sci. Technol. 47 (2), 140–169. https://doi.org/10.1080/10739149.2018.1493499.
Zheng, S., Ghandehari, M., Ou, J., 2016. Photonic crystal fiber long-period grating absorption gas sensor based on a tunable erbium-doped fiber ring laser. Sensors Actuators B Chem. 223, 324–332. https://doi.org/10.1016/j.snb.2015.09.083.
Zou, F., Liu, Y., Mou, C., Zhu, S., 2020. Optimization of Refractive Index Sensitivity in Nanofilm-Coated Long-Period Fiber Gratings Near the Dispersion Turning Point. J. Light. Technol. 38 (4), 889–897. https://doi.org/10.1109/JLT.5010.1109/JLT.2019.2949373.
Zubiate, P., Urrutia, A., Zamarreño, C.R., Egea-Urra, J., Fernández-Irigoyen, J., Giannetti, A., Baldini, F., Díaz, S., Matias, I.R., Arregui, F.J., Santamaría, E., Chiavaioli, F., Del Villar, I., 2019. Fiber-based early diagnosis of venous thromboembolic disease by label-free D-dimer detection. Biosens. Bioelectron. X 2, 100026. https://doi.org/10.1016/j.biosx.2019.100026.